Climate Dynamics (2022) 59:973–995
https://doi.org/10.1007/s00382-022-06168-6

Changes in extreme integrated water vapor transport on the U.S. west coast in NA-CORDEX, and relationship to mountain and inland precipitation

Mimi Hughes[1] · Dustin Swales[1,2] · James D. Scott[1,2] · Michael Alexander[1] · Kelly Mahoney[1] · Rachel R. McCrary[3] · Robert Cifelli[1] · Melissa Bukovsky[3]

Received: 3 May 2021 / Accepted: 24 January 2022 / Published online: 16 February 2022

Abstract
Western U.S. (WUS) rainfall and snowpack vary greatly on interannual and decadal timescales. This combined with their importance to water resources makes future projections of these variables highly societally relevant. Previous studies have shown that precipitation events in the WUS are influenced by the timing, positioning, and duration of extreme integrated water vapor transport (IVT) events (e.g., atmospheric rivers) along the coast. We investigate end-of-21st-century projections of WUS precipitation and IVT in a collection of regional climate models (RCMs) from the North American Coordinated Regional Downscaling Experiment (NA-CORDEX). Several of the NA-CORDEX RCMs project a decrease in cool season precipitation at high elevation (e.g., across the Sierra Nevada) with a corresponding increase in the Great Basin of the U.S. We explore the larger-scale controls on this terrain-related precipitation change in a subset of the NA-CORDEX RCMs through an examination of IVT-events. Projected changes in frequency and duration of IVT-events depend on the event's extremity: by the end of the century extreme IVT-events increase in frequency whereas moderate IVT-events decrease in frequency. Furthermore, in the future, total precipitation across the WUS generally increases during extreme IVT-events, whereas total precipitation from moderate IVT-events decreases across higher elevations. Thus, we argue that the mean cool season precipitation decreases at high elevations and increases in the Great Basin are largely determined by changes in moderate IVT-events which are projected to be less frequent and bring less high-elevation precipitation.

Keywords Mountain precipitation · Regional climate change · Atmospheric rivers

1 Introduction

Western U.S. (WUS) precipitation (and its resultant hydrologic impacts) critically affects the U.S. economy, because of its use in water resources and recreation (e.g., boating on reservoirs). It is also critical for U.S. ecosystems. WUS snowpack is also exceptionally vulnerable to anthropogenic climate change (McCrary et al. 2021; Fyfe et al. 2017; Knowles et al. 2006; Mote et al. 2005), thus motivating studies constraining climate model projections of precipitation (a necessary factor in snowpack projections) through physical process understanding.

Many papers have examined projected changes in WUS precipitation in global climate models (GCMs). Although uncertainty remains in the projected precipitation signal, we summarize the consistent results across these studies: Broadly, GCMs project a modest increase in wintertime precipitation (Neelin et al. 2013; Warner et al. 2015) which is more robust when using models identified as best-characterizing WUS precipitation and its controls (Langenbrunner and Neelin 2017) and also more robust for the northern U.S. west coast than for the southwest (Neelin et al. 2013). Extreme precipitation in general is projected to increase (Wuebbles et al. 2014), with indications that seasonality could be sharpened (i.e., the 'wet' season could be

✉ Mimi Hughes
mimi.hughes@noaa.gov

[1] Physical Sciences Laboratory, National Oceanic and Atmospheric Administration, Boulder, CO, USA

[2] Cooperative Institute for Research in Environmental Sciences, University of Colorado, Boulder, Boulder, CO, USA

[3] National Center for Atmospheric Research, Boulder, CO, USA

shorter) and relative frequency of extremely wet years could increase (Swain et al. 2018). For a more thorough overview of projected WUS precipitation changes, see Mahoney et al. (2021).

Integrated water vapor transport (IVT) is a strong control on cool season (October through March) WUS precipitation (Rutz et al. 2014; Dettinger et al. 2011; Neiman et al. 2008), especially in California (e.g., Ralph et al. 2006), where atmospheric rivers (ARs) account for over 50% of the annual total precipitation (e.g., Dettinger et al. 2011; Rutz and Steenburgh 2012). ARs are filaments of enhanced IVT often embedded within the warm sector of extratropical cyclones, and act as the primary synoptic mechanism for transporting moisture into western North America during the cool-season. Numerous methods, both objective/automated and subjective, have been used to identify ARs in the literature (see overview in Rutz et al. 2019). Most of these algorithms use either a fixed or a percentile-based threshold of IVT plus some additional geometry criteria to identify ARs. In this manuscript, we use a slightly broader metric with no geometry requirement that we call 'IVT-events'. These IVT-events represent a mixture of ARs as well as other oceanic-to-continental moisture transport atmospheric features that impact WUS precipitation (e.g., cut off lows; Abatzoglou 2016).

The characteristics of IVT-events (i.e., frequency, orientation, intensity, and duration) over a given watershed act as first-order controls on cool season precipitation amounts (e.g. Rutz et al. 2014; Dettinger et al. 2011): changes in the number of storms (IVT-event frequency), the IVT magnitude each storm brings (IVT-event intensity), and the dwell time of those storms (IVT-event duration) over a given watershed all impact the total amount of IVT incident on a watershed and thus available for precipitation. Increases in IVT-event frequency, intensity, or duration would all be expected to result in precipitation increases, if precipitation efficiency during IVT-events remained constant (e.g. Eidhammer et al. 2018). In addition, increases in IVT-event intensity and duration could potentially allow moisture to penetrate deeper into the interior of the WUS. IVT-event orientation impacts precipitation amounts and distribution in a less predictable way, with moderate shifts in orientation sometimes resulting in dramatic changes to precipitation over a given watershed (e.g., Hecht and Cordeira 2017; Picard and Mass 2017; Hughes et al. 2014); IVT-event orientation also emerges as a characteristic when IVT-events are grouped by other characteristics (e.g., 'wet' versus 'windy' ARs in Gonzales et al. 2020).

The Fifth Phase of the Coupled Model Intercomparison Project (CMIP5) projections suggest that Northern Hemisphere storm tracks will shift poleward (Chang et al. 2012). Since ARs are often embedded within extratropical cyclones (e.g., Payne et al. 2020), this shift of the storm track might cause a concomitant shift in AR frequency by latitude (Radic et al. 2015), although some studies of ARs note an equatorward shift (e.g., Shields and Kiehl 2016). Many papers have examined projected changes in AR frequency, intensity, and duration (Supplemental Table 1 lists several, along with a brief summary of results), sometimes in tandem with precipitation changes. Projected changes in IVT and ARs exhibit some consistent behaviors, with several studies (Rhoades et al. 2020; Payne and Magnusdottir 2015; Warner et al. 2015; Dettinger 2011) finding projected increases in WUS coast AR events, corresponding with an increase in future IVT (Lavers et al. 2015). This increase in IVT is largely caused by the increase in moisture in a warmer atmosphere, as changes in wind (dynamics) act to offset the increases in moisture (Gao et al. 2015). A recent review by Payne et al. (2020) summarizes the state of the science of ARs in a changing climate, including many of the salient mechanisms for changes in AR frequency, intensity, and duration, and resultant precipitation. They find AR-related precipitation will likely increase in intensity, but that projections are still uncertain because of the multiple scales (microscale to planetary) involved. Notably, few studies that investigate projected changes in ARs distinguish between ARs of different intensities.

While GCMs are necessary for projections of the global climate system, the complex terrain of the WUS is coarsely represented by the grid spacing of current-generation GCMs, leaving many of the processes that control precipitation in this region poorly resolved or absent entirely (Gutowski et al. 2020; Warner et al 2015; Hughes et al. 2014). These process limitations act both through direct and secondary processes. For example, elevation gradients of GCM terrain are generally too small, thus convergence and its resultant precipitation across GCM terrain is reduced (e.g., Smith et al. 2015). This too-small orographic precipitation then can result in too much moisture penetrating beyond initial mountain barriers into interior areas (e.g. Hughes et al. 2014). Regional climate models (RCMs) driven with boundary conditions from GCMs have demonstrated ability in adding value for precipitation processes in areas of complex terrain (e.g., Torma et al. 2015) while maintaining the large-scale synoptic features of their driving GCMs (Prein et al. 2019). The North American Coordinated Regional climate Downscaling Experiment (NA-CORDEX) downscales a subset of CMIP5 simulations (Table 1) to grid spacings of ~ 50 km and ~ 25 km. Current and future WUS NA-CORDEX precipitation have been evaluated (e.g., Gibson et al. 2019; Mahoney et al. 2021) and in general projections in NA-CORDEX were found to be consistent with previous CMIP5 results, but with terrain-controlled mesoscale details differing significantly in certain regions, for example the Sierra Nevada of California (Mahoney et al. 2021). The NA-CORDEX grid spacings of 25–50 km mitigate some but not all of the resolution-related issues with precipitation

Table 1 NA-CORDEX simulations used in this paper, sorted by GCM and RCM, with abbreviated GCM names as used in this manuscript (full GCM names are shown in Table S2). Adapted from a similar table available on https://na-cordex.org/simulation-matrix.html. Numbers in parentheses refer to the model numbers used in Fig. 3

	RCM					
	CanRCM4	CRCM5	RCA4	RegCM4	WRF	HIRHAM5
GCM						
Can	0.44° (5), 0.22° (16)	0.44° (4)	0.44° (6)			
EC			0.44° (7)			0.44° (12)
GFDL				50 km (8), 25 km (17)	50 km (2), 25 km (14)	
HadGEM				50 km (9), 25 km (18)	50 km (1), 25 km (13)	
MPI				50 km (10), 25 km (19)	50 km (3), 25 km (15)	
MPI		0.44° (11)				

processes (e.g., Hughes et al. 2014 found inland-penetration errors were reduced at 27 km grid spacing compared to 81 km, but < 10 km grid spacing was ideal).

This study examines changes in NA-CORDEX precipitation and changes in IVT-events (frequency, duration, and intensity) for a subset of NA-CORDEX simulations. It then relates the changes in those IVT-events to regional changes in precipitation in the WUS. Specifically, we address the following questions:

- What do projected changes in seasonal and sub-seasonal IVT, and in IVT-events, tell us about changes in cool season precipitation throughout the WUS?
- Are there differences in the projections for extreme versus moderate IVT-events?
- What are the physical reasons for WUS NA-CORDEX precipitation changes in terms of responses to moderate and extreme IVT-event characteristics (frequency, duration, and intensity)? How do these changes manifest at low- and high-elevation?

While many of the broader questions are addressed for the WUS as a whole, the projected precipitation changes and relationship to IVT-events is discussed in the context of three watersheds in the southwestern U.S.: the Sacramento, San Joaquin, and Central Nevada Desert Basin (CNDB) (Fig. 1). The Sacramento and San Joaquin basins were selected because of their relevance to water resources in California, as the two largest rivers in California (USBR 2016), while the CNDB is discussed because of its consistently positive projected precipitation changes.

2 Data and methods

2.1 NA-CORDEX and CMIP5

The CMIP5 (e.g., Taylor et al. 2012) multi-model ensemble archive is used in this manuscript to provide context for the NA-CORDEX experiments, which use CMIP5 simulations as their lateral boundary conditions. For this brief analysis of GCM precipitation projections (Fig. 1a, b), we compare results from the small (6 member) subset of CMIP5 simulations used as lateral boundary conditions for the NA-CORDEX RCMs to results from the broader CMIP5 ensemble (Bukovsky and Mearns 2020). For the latter, our analysis uses one ensemble member from 36 simulations in the CMIP5 archive. The full set of 36 CMIP5 simulations is listed in supplemental Table S2, and the six CMIP5 simulations used as lateral boundary conditions for NA-CORDEX experiments are noted with an asterisk in Table S2 and listed in Table 1.

The NA-CORDEX (Mearns et al. 2017) is the North American branch of the WCRP CORDEX initiative, which provides a framework for global regional climate modeling (RCM) activities (Giorgi et al. 2009; Gutowski et al. 2016). We use a subset of NA-CORDEX simulations (Table 1; see the current simulation matrix at https://na-cordex.org/index.html) that were available during our analysis period. We analyze precipitation from 19 NA-CORDEX simulations (at both ~ 50 km and ~ 25 km grid spacing), generated by a combination of 6 RCMs (CRCM5, RCA4, RegCM4, WRF, CanRCM4, and HIRHAM5) driven at

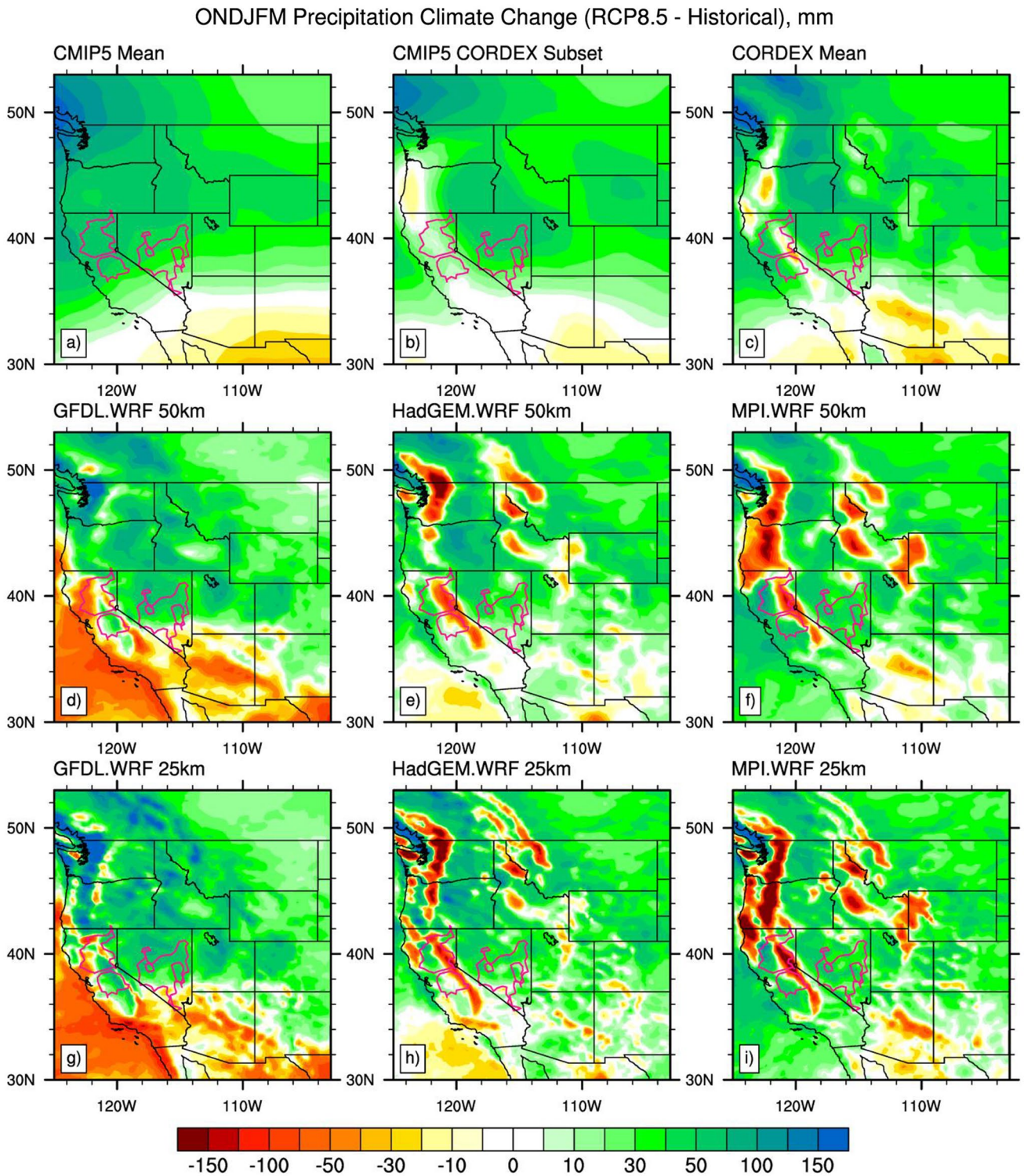

Fig. 1 **a** Cool season total mean precipitation change in mm (RCP8.5—historical) for CMIP5 ensemble. **b** Same as **a** except for five of six CMIP5 models used as boundary conditions for NA-CORDEX simulations (i.e., HADGEM2-ES, Can-ESM2, MPI-ESM-LR, MPI-ESM-MR, and GFDL-ESM2M). EC-EARTH is not included because no precipitation output was available. **c** Same as **a** but for NA-CORDEX ensemble. **d–f** Cool season total precipitation change in mm (RCP8.5—historical) for 50 km **d** GFDL.WRF, **e** HadGEM.WRF, and **f** MPI.WRF. **g–i** Cool season total precipitation change in mm (RCP8.5—historical) for 25 km, **g** GFDL.WRF, **h** HadGEM.WRF, and **i** MPI.WRF. Magenta contours outline three watersheds: Sacramento (top left), San Joaquin (bottom left), and Central Nevada River Basin (right)

their lateral boundaries by 6 CMIP5 GCMs (HadGEM2-ES, CanESM2, MPI-ESM-LR, MPI-ESM-MR, EC-EARTH, GFDL-ESM2M) as well as by ERA-Interim reanalysis (ERAi). Throughout the manuscript we use the naming convention of GCM.RCM for the NA-CORDEX simulations, abbreviating the GCM names as shown in Table 1; for example, the CanESM2-forced CRCM5 simulation is called Can.CRCM5. Due to the availability of model output, our IVT analysis focuses only on the 25 km WRF simulations, with some of the (qualitatively very similar) results for the 50 km WRF simulations shown in supplemental material. Raw output from NA-CORDEX simulations is not publicly available: The public archive does not host upper-level atmospheric variables because of their significant size (e.g., ~ 300 TB for WRF CORDEX simulations) and relative lower importance to most users (McGinnis and Mearns 2021), and our compute resources only allowed for the post-processing of this set of WRF simulations to which we had access.

For all analyses (i.e., CMIP5 and NA-CORDEX) we concatenate the historical scenario simulations (available 1950–2005 for NA-CORDEX and 1860–2005 for CMIP5) with the first 5 years of the RCP simulations (available 2005–2100) to create our 'historical' period (1980–2010), overlapping with the ERA-Interim-forced simulations; even though the last 5 years of our 'historical' period are technically the first 5 years of the RCP, the climate forcing during those 5 years is negligibly different from observations (Schwalm et al. 2020). CMIP5 and NA-CORDEX future climate simulations were run continuously from 2005 to 2100, but we analyze only the final 30 years of those simulations (2070–2100) as our 'future' period. CMIP5 includes several long-term (i.e., to 2100) experiments. NA-CORDEX simulations exist for both RCP 4.5 and 8.5, but far more simulations are available for RCP 8.5; therefore, for brevity we only present results from this more extreme emission scenario.

2.2 Observation-based precipitation

Observational estimates of historical precipitation are provided by a gauge-based, statistically gridded precipitation dataset, Newman et al. (2015). Several recent papers have documented large uncertainties in precipitation estimates across the WUS (Henn et al. 2018; Lundquist et al. 2019 and references therein), and Hughes et al. (2017) showed the Newman dataset underestimated windward Sierra Nevada precipitation during a recent water year; however, it represents one of the best-available estimates of WUS precipitation and thus is used for comparison to the historical RCM precipitation amounts.

2.3 Integrated water vapor transport (IVT)

IVT is calculated as:

$$IVT = -\frac{1}{g}\int_{p_0}^{p_{top}} q\boldsymbol{V}dp$$

where q is specific humidity, $\boldsymbol{V}$ is the horizontal wind vector, g is the acceleration of gravity, dp is the vertical thickness of each atmospheric layer, in pressure units, p_0 is the surface pressure and p_{top} is 50 hPa. IVT was calculated from the three available WRF GCM-forced simulations: HadGEM. WRF, GFDL.WRF, and MPI.WRF, and the ERAi-forced simulation, ERAi.WRF. The WRF model uses hybrid vertical coordinates and the IVT calculation was performed on WRF's native vertical grid (28 terrain-following levels, with ~ 10 to 80 hPa spacing below 500 hPa).

We investigate changes in IVT from three perspectives: (1) long-term seasonal and monthly mean IVT (calculated as the mean of the 3-h instantaneous values), (2) the estimated probability density functions (ePDFs) of 3-h IVT along the US west coast, and (3) frequency and duration of 'IVT-events'. The technique we use for identifying IVT-events is based on coastal IVT intensity and duration as follows: Histograms of IVT from the historical simulations are constructed for every WRF grid point along the U.S. west coast (Fig. 5a, inset), and used to identify historical IVT percentiles for each coastal location. These percentile values—for example, the 99th (90th) percentile of IVT for the grid point at ~ 37 N is 542 kg m^{-1} s^{-1} (259 kg m^{-1} s^{-1}) in ERAi.WRF—which vary greatly by latitude, are then used to identify 'IVT-events' with one additional criterion: IVT is required to exceed the threshold for at least 24 h for at least one gridpoint along the coast, which can move in time. We tested duration requirements ranging from 18- to 72-h at 6-h increments (not shown). As the duration requirement is lengthened, the number of IVT-events per season and the percentage of cool season precipitation the IVT-events contribute are reduced. Results are qualitatively similar for duration requirements from 18- to 48-h but for longer duration requirements the number of IVT-events/season becomes small making the detection of a climate change signal difficult. Overlapping hours exceeding the percentile threshold at adjacent grid points along the coast are combined, resulting in a 'catalog' of events that includes start and end times as well as start and end latitudes. Historical IVT thresholds are used to identify events for the future period. For IVT-event composites, we examine 'extreme' IVT-events (IVT > 99th percentile for at least one coastal grid point for at least 24 h) and 'moderate' IVT-events (90th < IVT < 99th percentile for at least one coastal grid point for at least 24 h).

Our definition of IVT-events is broadly similar to existing definitions for ARs (Shields et al. 2019), and many AR objective criteria use IVT thresholds close to the IVT threshold for our 'moderate' IVT-events. However, as noted above, our IVT-event definition is inclusive of some non-AR features (e.g., cutoff lows) since we have no geometry requirements: Imposing geometry requirements on west coast ARs in NA-CORDEX is somewhat problematic because of the limited western extent of the NA-CORDEX domain, which might 'trim' geometrically long ARs. Of the different AR identification metrics described in Ralph et al. (2019b), our method is local-percentile-based like Mundhenk et al. (2016), with a persistence criterion similar to Sellars et al. (2013). A method based on local percentiles has advantages to absolute-threshold-based methods (e.g., the water-resources-relevant AR categories—AR Cats—of Ralph et al. 2019a) when comparing across multiple GCMs or RCMs, because it effectively normalizes for changes in IVT with latitude and for model-dependent base-state biases. Nevertheless, because of its relevance to water resources, the percentiles that correspond to the AR-Cat 1–5 thresholds in ERAi.WRF and MPI.WRF at several latitudes are shown in Tables S3 and S4.

3 Results

3.1 Projections of precipitation

The goal of this manuscript is to investigate the interplay between changes in WUS IVT and precipitation in NA-CORDEX; the first step to that goal is describing the precipitation changes themselves.

3.1.1 CMIP5

Here we compare the ensemble mean of five of the six CMIP5 simulations used as lateral boundary conditions in NA-CORDEX to the larger 36-simulation CMIP5 ensemble mean; EC-EARTH is not included because its precipitation data were not available.

The mean CMIP5 (36 GCMs) projected change in cool season precipitation shows an increase of 20–50 mm (~ 10% of the cool season total precipitation amounts for most of the region, not shown here but, e.g., see Chapter 7 of Wuebbles et al. 2017) for locations north of ~ 35 N, and decreased precipitation south of this latitude (Fig. 1a). The magnitude of the projected increase is larger at higher latitudes and along the coast. Individual simulations generally agree with increased northern precipitation (not shown), but the location of the sign change for precipitation projections is model-dependent (Neelin et al. 2013). No evidence of terrain sensitivity is evident in the GCM mean projected changes.

Narrowing the CMIP5 ensemble to include only those simulations used as boundary conditions for the NA-CORDEX simulations (i.e., HADGEM2-ES, Can-ESM2, MPI-ESM-LR, MPI-ESM-MR, and GFDL-ESM2M) (Fig. 1b), reveals that, like for the full CMIP5 ensemble, much of the WUS has projected increases in precipitation in the CMIP5 subset. However, unlike the full CMIP5 ensemble, the NA-CORDEX subset shows a dipole with respect to coastal and inland precipitation changes in the Pacific NW. On the western side there is a decrease in precipitation extending from the WA-OR border southward along the high-Cascades to the Northern extent of the CA Central Valley, whereas further inland, we see a local maximum. The GCMs selected as forcings for NA-CORDEX span the range of global climate sensitivity (Bukovsky and Mearns 2020), but as is apparent in this figure, are not necessarily representative of the full CMIP5 ensemble in terms of their regional precipitation response. In addition, some of these regional differences likely arise due to internal variability (Deser et al. 2012), that are more apparent with the smaller model sample size.

3.1.2 NA-CORDEX

In general, the higher resolution in NA-CORDEX simulations results in a more realistic representation of precipitation over terrain than in the CMIP5 simulations (Figure S1 and Mahoney et al. 2021), and thus a natural question is, how does the projected precipitation change in NA-CORDEX compare with the change from its set of driving GCMs?

The multi-model NA-CORDEX RCM cool-season precipitation changes (Fig. 1c) are similar to those seen in the NA-CORDEX CMIP5 subset (Fig. 1b) with a regional mean increase north of ~ 35 N, but with greater detail and some localized decreases over the complex terrain of the region. Unlike the GCM-subset precipitation changes, decreases in precipitation are larger across the highest terrain of the Cascades, Sierra Nevada, and Mogollon Rim of AZ, with smaller decreases along the coast near the CA/OR boundary. In the northern interior states, localized precipitation-change maxima follow the lowest terrain (e.g. Columbia and Snake river valleys), while localized minimums of increased precipitation are isolated to the highest terrain (e.g. Sawtooth range in ID, or the Wasatch range in UT). The largest regional increases occur in the Pacific Northwest, whereas the largest regional decreases occur in the southernmost portions of the domain.

Inspection of individual simulations (Figure S3 and Fig. 1d–i) reveals that most simulations project an increase in cool season precipitation over much of the WUS, with localized decreases; the GFDL and EC simulations have the largest areas of decreases in the southernmost states. The historically very dry regions inland of the Sierra Nevada and Cascades (i.e., Nevada, eastern Washington, and eastern

Oregon) exhibit increased precipitation of 10–30 mm in nearly all simulations, which results in upwards of a 20% increase in cool season precipitation in some models and months (not shown; see Mahoney et al. 2021 or https://psl.noaa.gov/ipcc/cordex/). Variations in the multi-model mean are related to fine-scale variations both of magnitude and change in the individual simulations: all except one NA-CORDEX simulation projects a decrease in cool season precipitation for at least one mountainous region of the WUS, often adjacent to an increase at lower-elevations. For example, the Sierra Nevada have projected decreases in 14 of the 19 simulations, with projected increases in the Central Valley of CA for many of these simulations. The magnitude and exact location of these projected decreases varies from simulation to simulation, reflecting sensitivity to both the lateral forcing data and to sub-grid-scale physics parameterizations in these models. As the necessary data to calculate IVT was only available from the WRF simulations, we now focus on their precipitation changes (Fig. 1d–i): the WRF simulations exhibit moderate changes in precipitation compared with some other NA-CORDEX simulations, but all exhibit some reductions in precipitation across the higher elevations of the Sierra Nevada flanked by increases to the northeast and southwest of the Sierra Nevada (albeit with larger variations across other parts of the WUS); this pattern is less clear in the GFDL.WRF simulations than in the HadGEM.WRF and MPI.WRF simulations.

We next examine the seasonality of the projected cool season changes for three Hydrologic Unit Code, level 4 (HUC 4; USGS and USDA 2013) watersheds in California and Nevada: The Sacramento River basin (HUC4 subregion 1802), the San Joaquin River basin (HUC4 subregion 1804), and the Central Nevada Desert Basins (CNDB, HUC4 subregion 1606). Figure 1 displays locations of the basins (and Figure S2 displays the locations on the RCM grids). The observation-based seasonal cycle of precipitation in the Sacramento watershed increases to a broad December–January–February peak, although

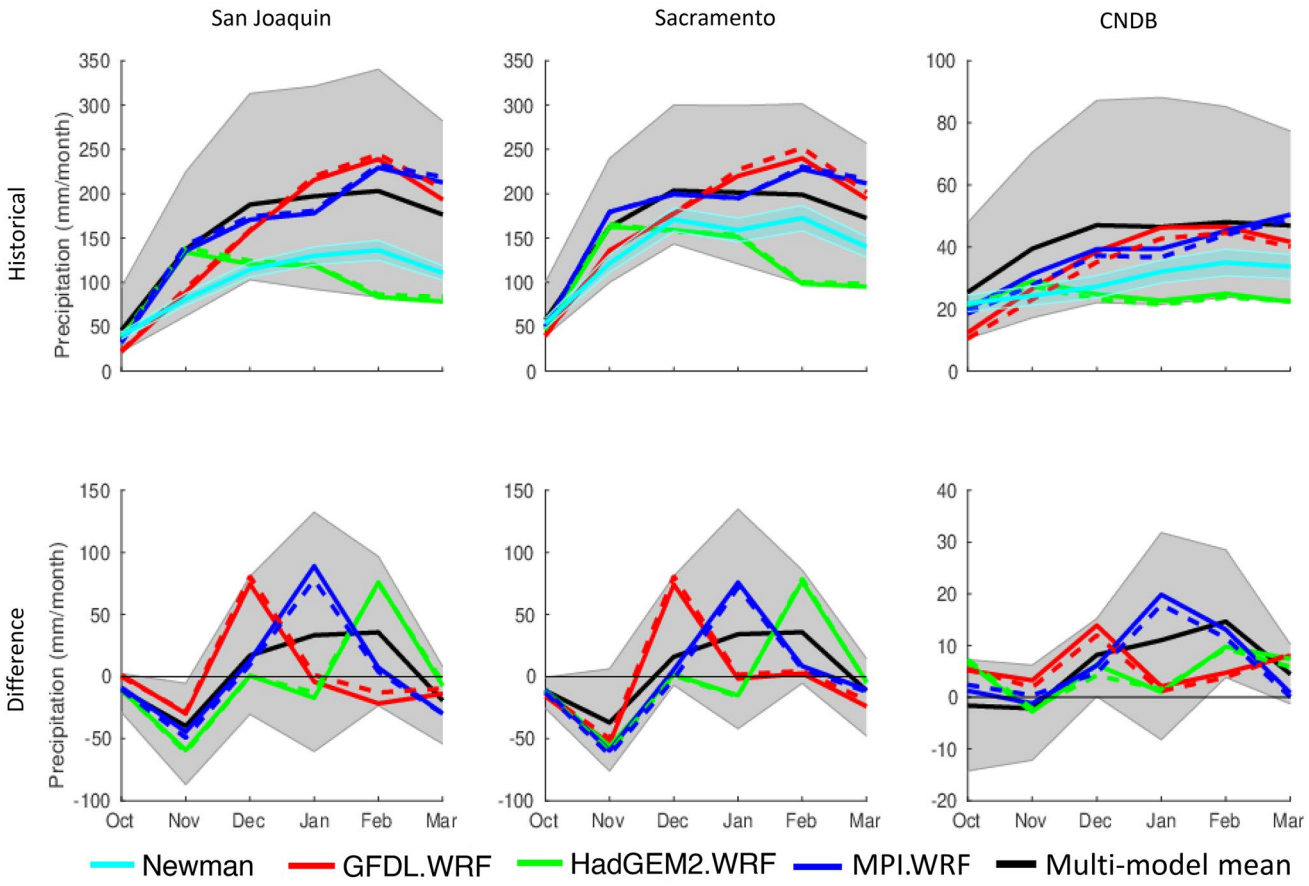

Fig. 2 (top) Historical mean, and (bottom) difference (RCP8.5-historical) in monthly mean precipitation for (left) San Joaquin watershed, (middle) Sacramento watershed, and (right) CNDB watershed. Black line shows NA-CORDEX multi-model mean, and grey shaded region shows full range (minimum to maximum). Cyan line (shading) shows Newman mean (±1 standard deviation). Red/green/blue lines show values from GFDL.WRF, HadGEM.WRF, and MPI.WRF, respectively, with solid lines for 50 km simulations and dashed lines for 25 km simulations. Locations of watersheds are shown on Fig. 1. The y-axis range is much smaller for the CNDB

significant amounts of precipitation fall during October, November, and March (Fig. 2); the same is largely true for the San Joaquin although with a more well-defined February maximum. CNDB receives much less precipitation than the two CA watersheds, and the monthly variation in precipitation is also smaller in magnitude, with an observations-based maximum in February similar to the San Joaquin. The NA-CORDEX simulations exhibit comparable seasonal cycles in all three watersheds relative to observations, although some simulations shift the maximum precipitation a bit earlier/later in the season (e.g. HadGEM2.WRF has a November maximum), and most of the simulations are positively biased in their monthly precipitation amounts (although it is also possible that the observations-based dataset underestimates precipitation at the highest elevations; Lundquist et al. 2019; Hughes et al. 2017). The 25 km WRF simulations tend to have slightly more precipitation than their 50 km counterparts in the Sierra Nevada watersheds, and about the same or slightly less precipitation in the CNDB (not shown for other models).

For the two California watersheds, projected changes in mean monthly precipitation (Fig. 2, bottom row) exhibit large model-to-model and month-to-month variability in both the magnitude and sign of the change. Nearly all simulations project a decrease in November precipitation, with an increase in one midwinter month, and the WRF simulations are representative of this general behavior: this results in a multi-model mean with a broad rather moderate midwinter increase and November decrease. Areal-average changes in the two CA watershed are similar in character, but larger, than those shown for all of CA in Mahoney et al. 2021. Projected mean monthly precipitation changes across the CNDB are more consistently positive, though still with large model-to-model variability in the timing of largest increases. These time series do not reveal the reason for the localized projected cool season decreases visible on the change maps.

To identify if localized projected cool season decreases are related to the terrain, we examine precipitation changes across the two California watersheds (binned together to increase the number of gridpoints in each boxplot) for gridpoints above and below 800 m (Fig. 3). The results were

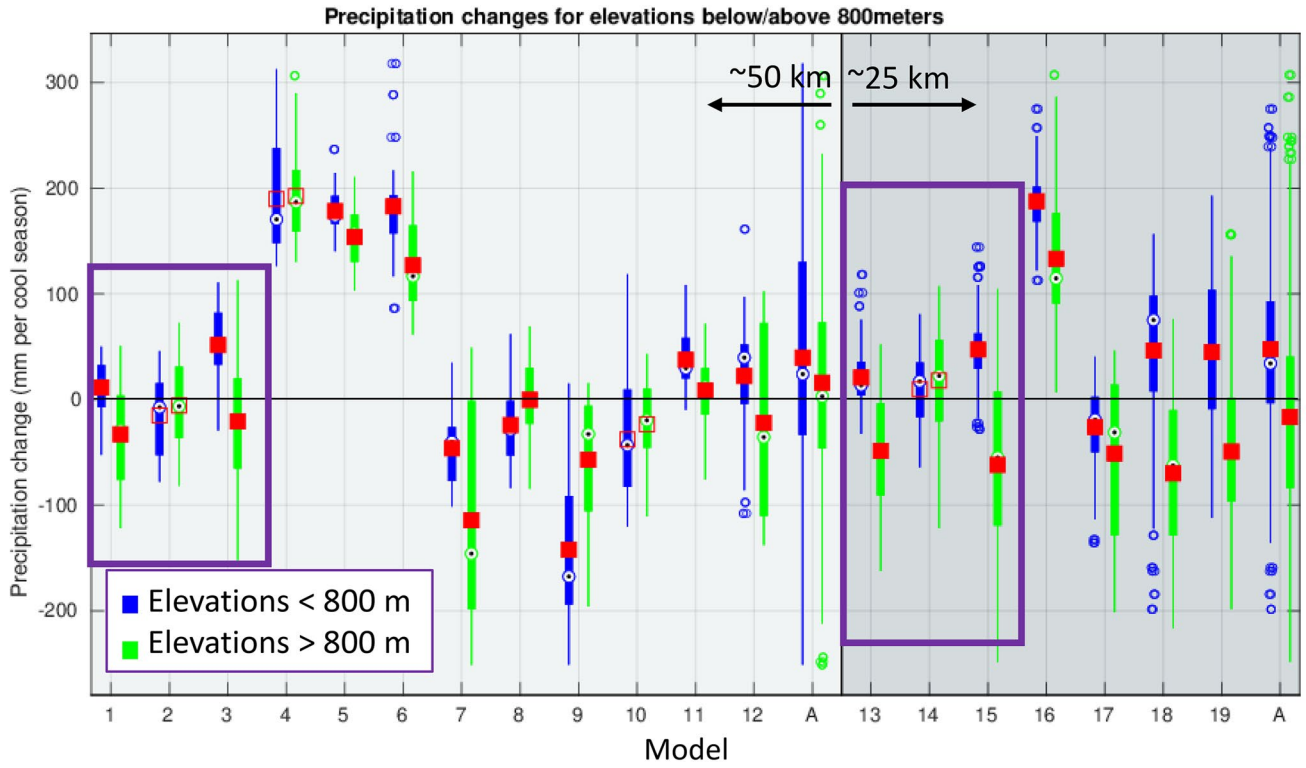

Fig. 3 Total cool season precipitation changes for gridpoints in the two California watersheds for each NA-CORDEX model (labeled 1–19, legend is shown in Table 1). Models 1–12 (light gray shaded background) have ~ 50 km grid spacing and models 13–19 (darker gray shaded background) have ~ 25 km grid spacing. Aggregate changes for the ~ 50 and ~ 25 km models (grouped separately) are shown with the bar groups labeled 'A'. HadGEM.WRF, GFDL.WRF, and MPI.WRF are models 1–3 and 13–15 for 50 km and 25 km grids, respectively, and are outlined with purple boxes. Each model has two box/whisker plots: the left (blue boxes) is gridpoints with elevations below 800 m and the right (green boxes) is gridpoints with elevations above 800 m. Open circles with black dots show median, boxes show 25/75 percentiles, whiskers extend to data points not considered outliers and small open circles show outliers. Red squares show means and are filled in for low/high elevation pairs that have significantly different means using a 2-sided t-test with 95% confidence intervals

not sensitive to the specific elevation threshold (thresholds between 800 and 1500 m were tested); we use the modest threshold of 800 m because a few 50 km simulations have very few truly 'high elevation' points. These box-and-whisker plots confirm that many of the localized precipitation decreases occur at high elevations. 7 of the 12 ~50 km resolution and 6 of the 7 ~25 km NA-CORDEX simulations have reduced changes at elevations above 800 m than for elevations between 0 and 800 m. In 7 of the 19 simulations this results in mean increases at lower elevations and mean decreases at higher elevations, whereas for 6 of 19 simulations the shift results in either a less positive or more negative mean precipitation change at higher versus lower elevations. The HadGEM.WRF and MPI.WRF simulations exhibit this behavior whereas the GFDL.WRF simulations do not have a noticeable (or statistically significant) difference in projected precipitation changes with elevation. The elevation changes are also larger for the ~ 25 km simulations than the ~ 50 km simulations, suggesting this behavior is sensitive to resolution of the underlying terrain.

3.2 Projections of IVT

As noted in the introduction, IVT is a primary control on cool season precipitation for the WUS. Here we examine changes in both mean IVT and 'IVT-events' (defined in "Integrated water vapor transport (IVT)") in the WRF NA-CORDEX simulations, which had 3D atmospheric variables available at 3-h temporal resolution. Results for the 25 km simulations are shown in the main text, while results for the 50 km WRF simulations are included in the supplemental material. We focus first briefly on changes in mean IVT, because of its relationship to the larger-scale storm tracks, and because it has been investigated in the literature (e.g. Lavers et al. 2015; Warner et al. 2015). We then examine changes in IVT-events, and investigate the relationship between changes in IVT-events and precipitation.

3.2.1 Bulk changes in distribution and seasonality

The cool season mean IVT in the ERAi.WRF simulation (Figure S4) strongly agrees with IVT from ERAi (not shown; c.f. Fig. 1 of Lavers et al. 2015) with a maximum in the northeastern Pacific Ocean, which is near the regional maxima of 850 hPa relative vorticity cyclonic storm track statistics (e.g. Bengtsson et al. 2006). Mean historical cool season IVT in the three GCM-forced NA-CORDEX WRF simulations is qualitatively similar to ERAi.WRF (Figure S4), although the magnitude and spatial extent of the enhanced IVT region varies slightly among simulations. All three simulations project increases in IVT in the future of up to 70 kg m^{-1} s^{-1}. These cool season increases in mean IVT are consistent with the results of Lavers et al. (2015), who found increases of 30–40% of DJF IVT in the CMIP5 ensemble.

Similar to the monthly changes in precipitation for the three watersheds, the projected changes in IVT are not constant across the months of the cool season (Fig. 4). IVT

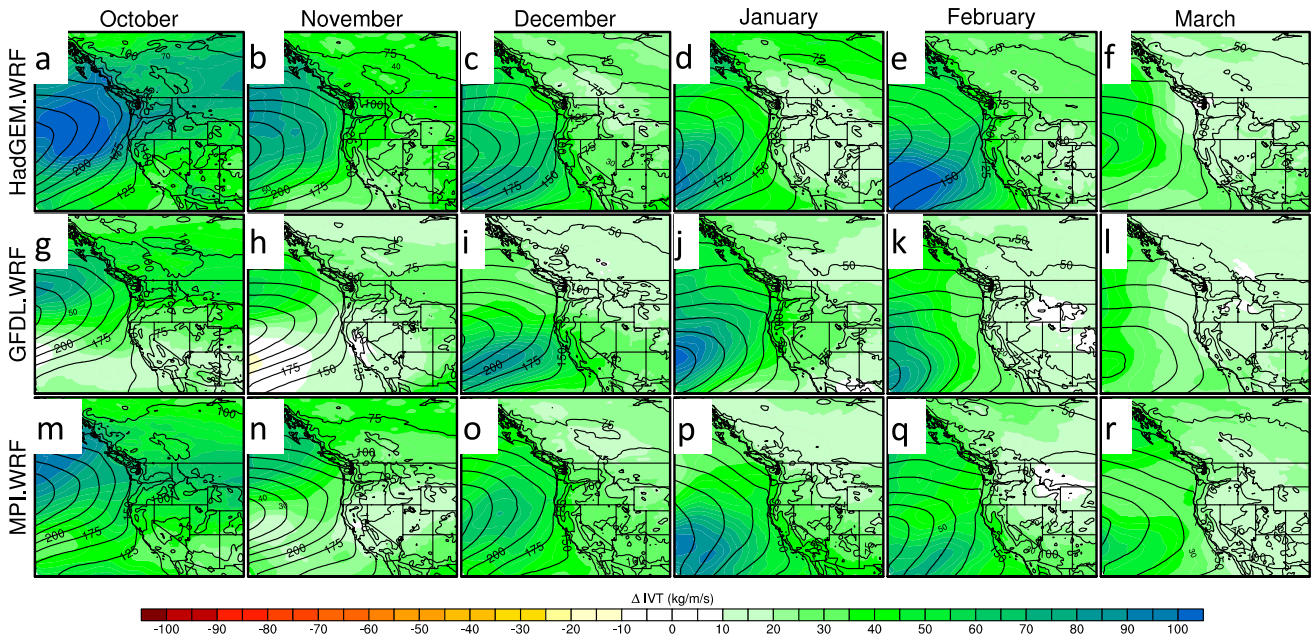

Fig. 4 Change (RCP8.5-historical) in mean monthly IVT (color fill) for each cool season month (columns) and for each 25 km WRF simulation (rows). Historical IVT is shown in the black contours, contoured every 25 kg m^{-1} s^{-1}

patterns begin the cool season with a maximum that intersects the west coast near the U.S./Canada border. This maximum migrates south as the cool season progresses; although all three simulations are qualitatively similar in this regard, there are subtle variations in exactly where the IVT maximum intersects the U.S. west coast each month. Projected changes are generally largest in the vicinity of the historical IVT maximums for each month, sometimes aligning with the historical IVT maximums (e.g., Fig. 4a) indicating an intensification of the historical spatial distribution, or sometimes flanking the maximum values (e.g., Fig. 4c) indicating a broadening of the historical spatial distribution. Large IVT increases in all three simulations occur during Oct-Nov. However, these increases occur to the north of the historical IVT maximum (e.g. GFDL.WRF; Fig. 4g, h), suggesting that increased storminess in these months would occur too far north to impact most of the WUS. By mid-winter the storm-track has moved south, and intensified with respect to historical simulations. The locations of projected changes also migrate southward as the cool season progresses resulting in the largest IVT increases near the coast of California that approximately align with the timing of largest precipitation changes for each WRF simulation.

We next examine the estimated probability distribution functions (ePDFs) of 3-hourly instantaneous IVT along the U.S. west coast, and discuss how the three WRF NA-CORDEX simulations project coastal IVT ePDFs will change in the future (Figs. 5 and S6). We construct these ePDFs for all coastal points, across all three simulations, with ePDFs for the ERAi.WRF simulation shown for reference (Fig. S5). Historical IVT ePDFs have their peak value below approximately 100 kg m^{-1} s^{-1}, and are positively skewed, with values > 500 kg m^{-1} s^{-1} occurring at northern west coast locations). The skewness is greater at northern than

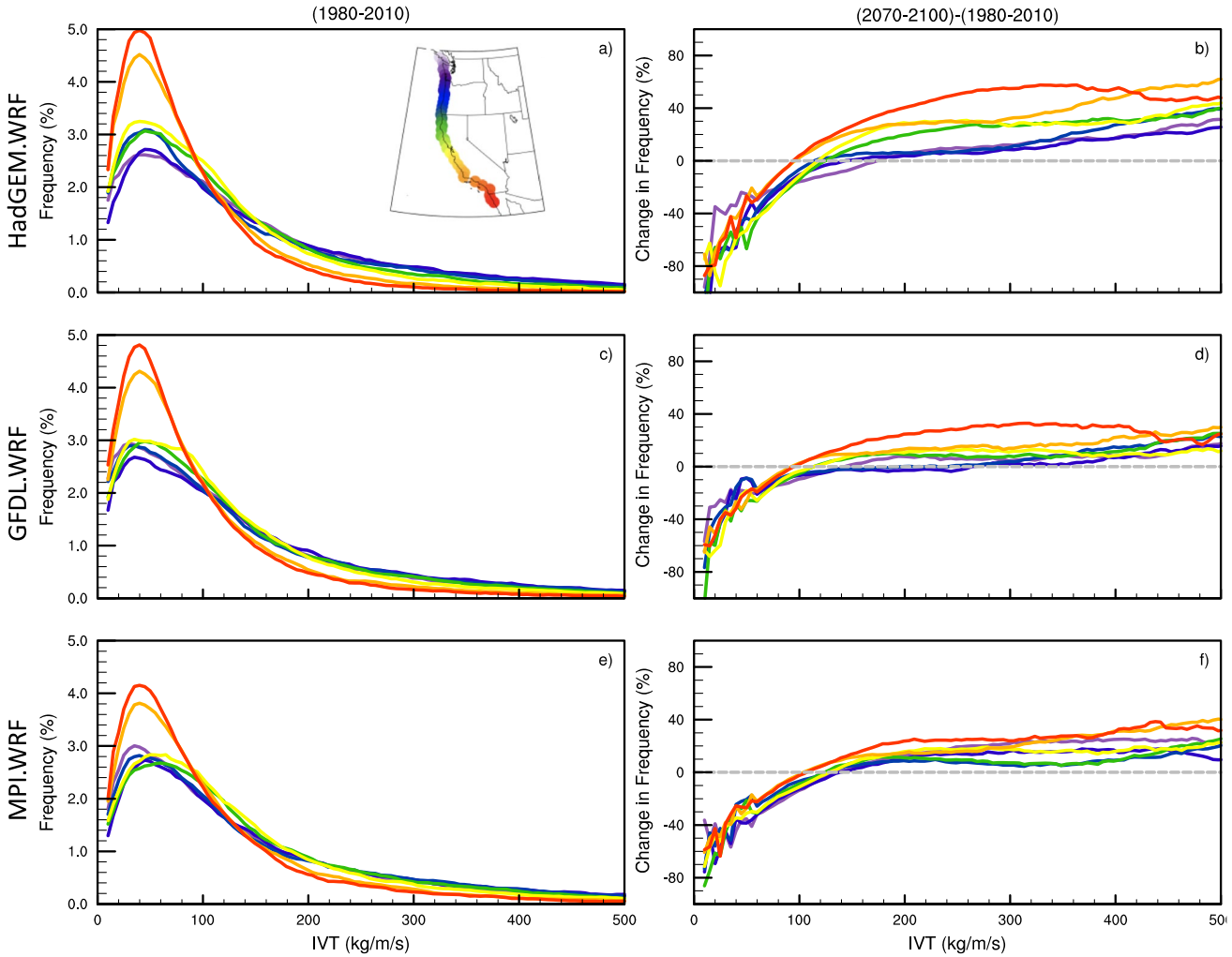

Fig. 5 Estimated probability distribution functions (ePDF) of cool-season (ONDJFM) integrated water vapor transport (IVT) sampled every 3 h at coastal locations (inset panel a) during: **a**, **c**, **e** historical and **b**, **d**, **f** difference (i.e., future-historical) in IVT ePDF, for **a**, **b** 25 km HadGEM.WRF, **c**, **d** 25 km MPI-ESM-LR.WRF, **e**, **f** 25 km GFDL.WRF. Inset in **a** shows locations of coastal gridpoints

southern latitudes. Proximity to the storm track may explain how these ePDFs change with latitude: Southern locations have fewer landfalling extra-tropical cyclones, resulting in fewer high IVT instances. The latitudinal structure of the ePDFs (visualized as the differences in the different colored lines on Fig. 5a) varies across the simulations, with MPI. WRF having the least meridional variation in the historical simulations.

All three WRF NA-CORDEX simulations project a shift in future IVT distributions at the coast: IVT values less than ~ 100 kg m^{-1} s^{-1} decrease in frequency at all latitudes in all three simulations, with an increase at higher IVT values. The largest increases are at the lowest latitudes, and smallest changes generally occur at higher latitudes. The general increases for IVT values above 200 kg m^{-1} s^{-1} are generally consistent with Warner et al. (2015) who found an increase in the 99th percentile west coast IVT values in 10 RCP8.5 CMIP5 models.

3.2.2 IVT-events: changes in frequency and duration

In the previous section we examined how the localized distributions of "instantaneous IVT" vary along the WUS coast and its response to a projected warming scenario. Here we examine the distribution of IVT-events, defined as persistent IVT anomalies incident on the coast using a Lagrangian approach where we track the IVT anomaly along the coast throughout the simulation. Results for these IVT-events differ from those for mean seasonal IVT and 3-h IVT because IVT is required to remain above the percentile-defined thresholds for at least one coastal gridpoint for at least 24 h, indirectly implying these IVT-events are caused by larger-scale forcing (e.g., they could represent extratropical cyclone-induced ARs or cutoff lows near the coast). For much of the remaining analysis, we categorize IVT-events into two groups: events where IVT exceeds the historical 99th percentile at contiguous coastal gridpoints for a minimum of 24 h, hereafter 'extreme IVT-events', and events where IVT exceeds the historical 90th percentile but is below the historical 99th percentile at contiguous coastal gridpoints for a minimum of 24 h, hereafter called 'moderate IVT-events'. Based purely on the number of days per cool season, a 99th percentile IVT value would occur a little less than twice per cool season and a 90th percentile IVT value would occur 10% of the time or ~ 18 days in the historical cool season; the Lagrangian approach means the moderate and extreme IVT-events can happen somewhat more frequently than this lower limit, since the threshold need only be exceeded at one gridpoint along the coast that can change over the course of each event.

To confirm that these IVT-events are relevant for understanding changes in cool season precipitation, we first examine the contribution of IVT-events to cool season mean precipitation in the historical simulations (Figs. 6 and S7), similar to existing examinations of the precipitation contribution of U.S. west coast ARs (Dettinger et al. 2011; Rutz et al. 2014; Ralph et al. 2019b). Extreme IVT-events account for upwards of 30 percent of the total cool season precipitation (Fig. 6, center), with the largest values in California's mountains. Moderate IVT-events contribute to an even larger fraction of cool season precipitation (Fig. 6, left), and the combination of moderate and extreme IVT-events (Fig. 6, right) accounts for a very large fraction of cool season precipitation in the WUS (~ 80% across much of California). The three GCM-forced WRF simulations and ERAi.WRF have very similar patterns of percent contribution to cool season total precipitation.

We next investigate the changes in cool season IVT-event frequency as a function of event threshold percentile (Fig. 7). All three GCM-driven WRF simulations have IVT-event frequency similar to ERAi.WRF's frequency; GFDL.WRF differs the most from ERAi.WRF as it contains consistently more IVT-events at all IVT thresholds (Fig. 7a). IVT-events for thresholds below about the 98th% are reduced in frequency by approximately 0.5–3 events/cool season in all three simulations. HadGEM.WRF and MPI.WRF have an increase in the number of IVT-events with event thresholds above the 99th% of approximately 1 event/year, which is large given these more extreme IVT-events happen fewer than 3 times per year in the historical simulations; GFDL.WRF has smaller changes in event frequency for event thresholds above the 99^{th}%. Thus, despite increases in the monthly mean IVT in nearly all cool season months (Fig. 4 and Figure S4), the frequency of moderate IVT-events decreases in all three WRF simulations, and the frequency of extreme IVT-events increases.

3.3 IVT-event changes in IVT and impact on precipitation

This section explores the changes in moderate and extreme IVT-events further, by examining how composite IVT and precipitation change during extreme and moderate IVT-events. Table 2 provides the number of 3-hourly instances of moderate and extreme IVT-events that go into each composite (Table S5 shows the number of events that go into each composite): consistent with Fig. 7, the number of hours during extreme IVT-events increases and the number of hours during moderate IVT-events decreases in all three WRF simulations. We note that since our analysis uses historical IVT thresholds to identify IVT-events, it potentially convolves changes in storminess (e.g., fewer/more extratropical cyclones) with changes in storm intensity; we leave the reasons for changes in IVT-events to future work.

The historical composite IVT (Fig. 8, contours) for moderate IVT-events has a broad, westsouthwest-to-eastnortheast

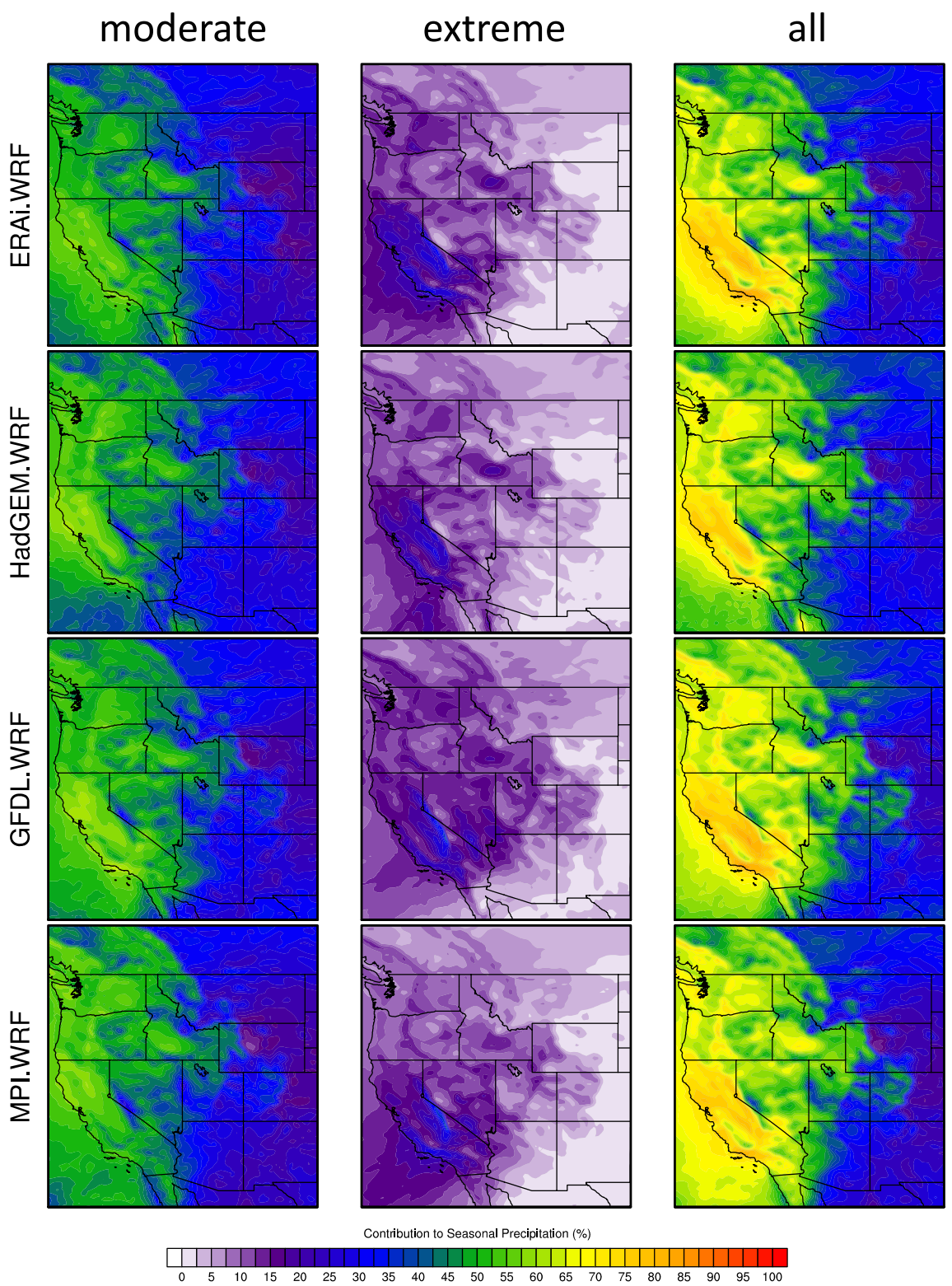

Fig. 6 Contribution to cool season total precipitation associated with (left) moderate IVT events, (center) extreme IVT events, and (right) all IVT events in (top) ERAi.WRF, (second row) HadGEM.WRF, (third row) GFDL.WRF, and (bottom) MPI.WRF in 25 km WRF simulations

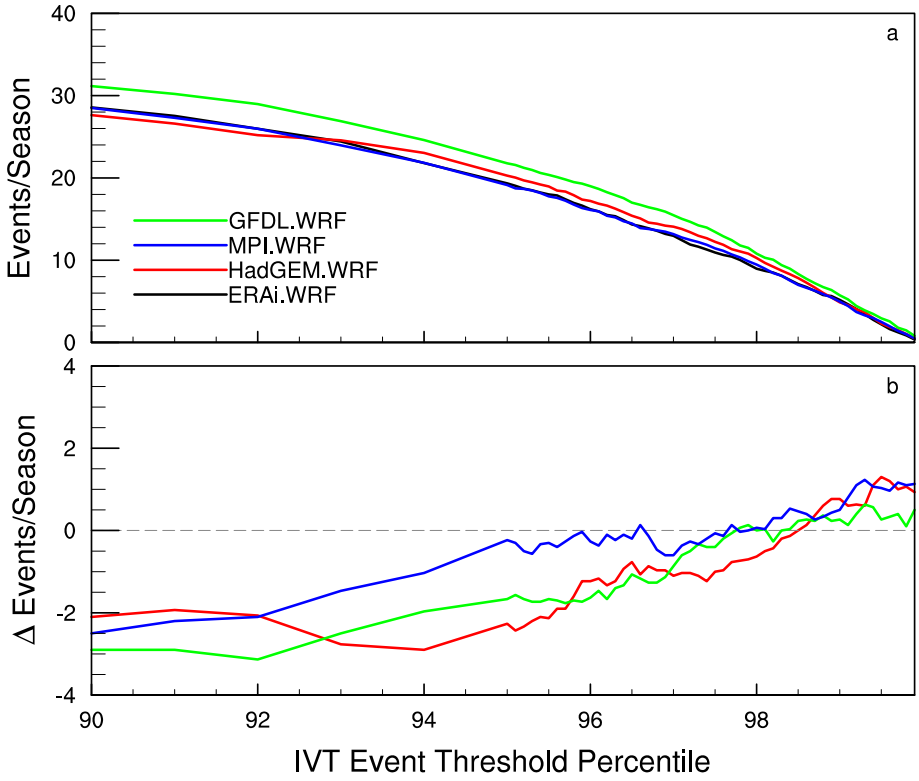

Fig. 7 Cool-season (ONDJFM) 24-h IVT event statistics for historical and future simulations for IVT events along entire western US coastline in 25 km WRF simulations, as a function of IVT event threshold percentile. **a** Historical IVT event statistics for GFDL.WRF, MPI.WRF, HadGEM.WRF, and ERA-I.WRF. **b** Future-Historical IVT event statistics

Table 2 Number of 3-h instances during IVT-events in each model for the historical and future periods, and percent difference

	HadGEM.WRF	GFDL.WRF	MPI.WRF
Extreme (99th)			
Historical	1863	2250	1709
Future	2236	2303	2019
Percent change (Future–Historical)	+20%	+2%	+18%
Moderate (90th < IVT < 99th)			
Historical	15,084	15,866	14,845
Future	12,488	13,408	12,628
Percent change (Future–Historical)	− 17%	− 15%	− 15%

These are the number of instances in the composites of Figs. 8, 9, and 10

maximum that intersects the coast at approximately the CA/OR border in all three simulations. The historical composite IVT for extreme IVT-events similarly has a southwest-to-northeast tilted maximum offshore, but the maximum is much greater (by definition), and the 'landfall' position varies more from simulation to simulation. The offshore orientation of the historical composites also varies across simulations more in the extreme events than for the moderate events. The broader maximum in the moderate IVT-event composite is likely a result of the much larger number of instances in this composite.

The projected changes in composite IVT-event IVT (Fig. 8, color fill) are positive everywhere in the domain. This shift is consistent with the projected shift in mean IVT (Figs. 4 and S4), and occurs despite reductions in the frequency of moderate IVT-events; thus the number of moderate IVT-events is reduced while their average intensity (i.e., mean IVT field) increases. The spatial distribution of the changes varies considerably by simulation and event threshold: HadGEM.WRF exhibits increases approximately co-located with the historical maximum for moderate IVT-events, but increases southwest and northeast of the historical maximum for extreme IVT-events. GFDL.WRF also exhibits increases co-located with the historical maximum for moderate IVT-events, but the increases for extreme IVT-events are on the southeastern and northwestern side of the historical maximum. MPI.WRF's increases stretch from southwest to northeast for both event types. Future increases co-located with the historical maxima indicate intensification, whereas increases shifted off-center from historical

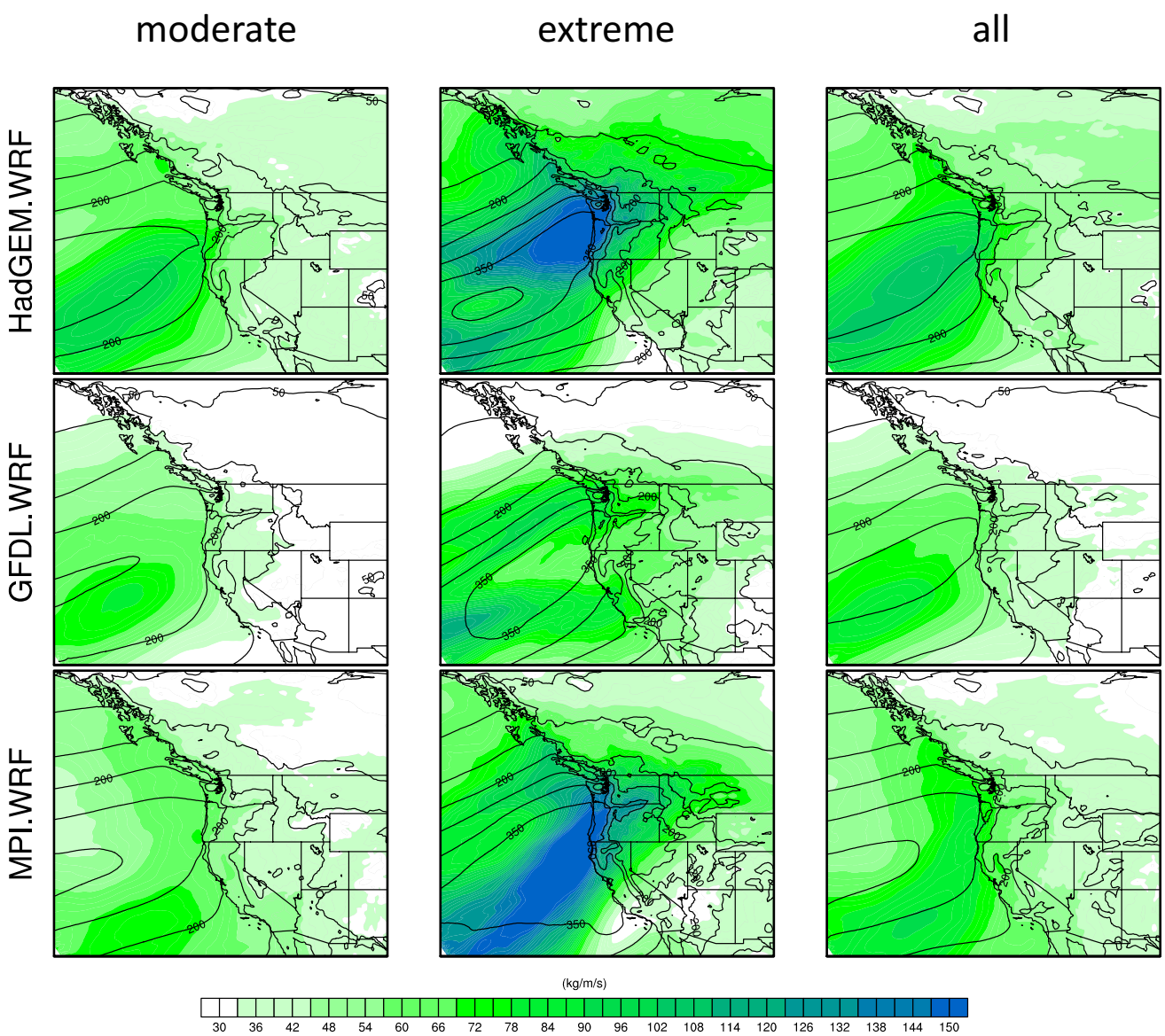

Fig. 8 Change (future–historical, as color fill) in mean IVT during (left) moderate IVT events, (center) extreme IVT events, and (right) all IVT events in (top) HadGEM.WRF, (middle) GFDL.WRF, and (bottom) MPI.WRF in 25 km WRF simulations. Black contours show historical mean IVT event IVT contoured every 50 kg m^{-1} s^{-1}. These composites are for all ONDJFM IVT events of each type

maxima imply a change in orientation, which is discussed further in "Discussion".

Composites of IVT-event precipitation rate (Fig. 9) also have changes that vary with simulation. In all three simulations moderate IVT-events show mostly small positive or near zero changes across most of the WUS, except for decreases in the northern Cascades in HadGEM.WRF, decreases in the Los Angeles area and Mogollon rim of AZ in GFDL.WRF, and decreases in the southern Cascades and mountains of Idaho in MPI.WRF. Extreme IVT-events generally exhibit large localized changes in precipitation rate that vary across simulations and map to the regions with the largest changes in composite event IVT: HadGEM.WRF and MPI.WRF have large precipitation rate increases in the Pacific NW, corresponding with the SW to NE increases in extreme event composite IVT, whereas GFDL.WRF has the largest precipitation rate increases along the Sierra Nevada, corresponding with the more zonally oriented composite IVT increases.

The precipitation rate changes for the moderate IVT-events are small compared to precipitation rate changes during extreme IVT-events. However, moderate IVT-events occur 6–8 times as often (Table 2), so to understand the relative impact on cool season precipitation we next compare the change in total precipitation (divided by 30 so that it has units of mm per-cool-season) from the two types of

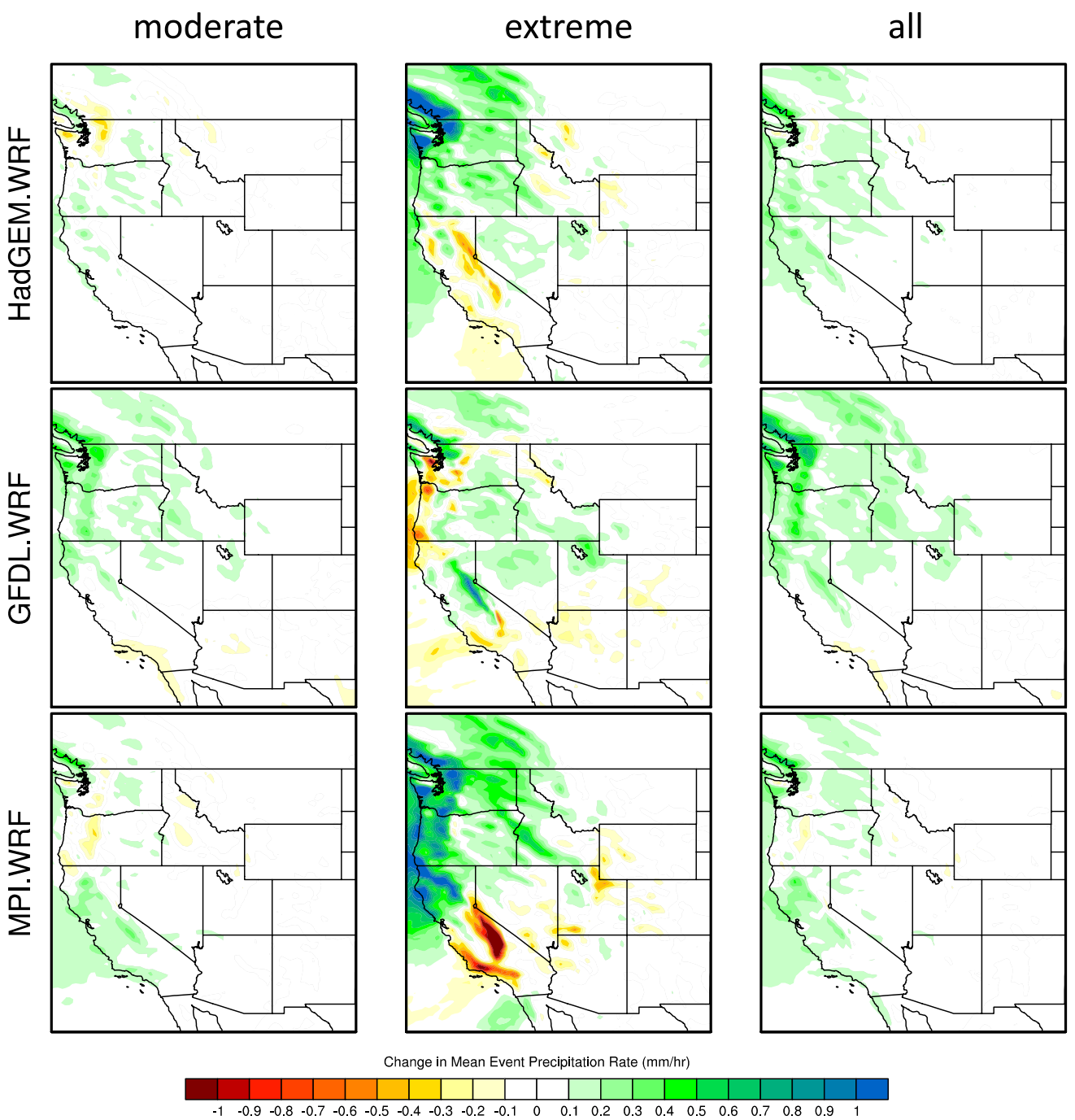

Fig. 9 Change (future–historical) in mean precipitation rates during (left) moderate IVT events, (center) extreme IVT events, and (right) all IVT events in (top) HadGEM.WRF, (middle) GFDL.WRF, and (bottom) MPI.WRF in 25 km WRF simulations

events (Fig. 10). Here a clear picture emerges across all three simulations: extreme IVT-events generally produce precipitation increases across most of the WUS, particularly across the Cascades and the northern Sierra Nevada. In contrast, moderate IVT-events have large decreases across much of the higher terrain of the WUS, with modest increases in a few locations (most consistently across simulations in areas of Utah, and eastern WA and OR). The net effect of the two types of events (i.e., 'all' column of Fig. 10) to a large degree aligns with the cool season mean precipitation changes for each simulation (Fig. 1 g–i): although the exact patterns vary across simulations, each simulation has localized decreases at higher elevations amidst increases across much of the rest of the WUS. In addition, when these

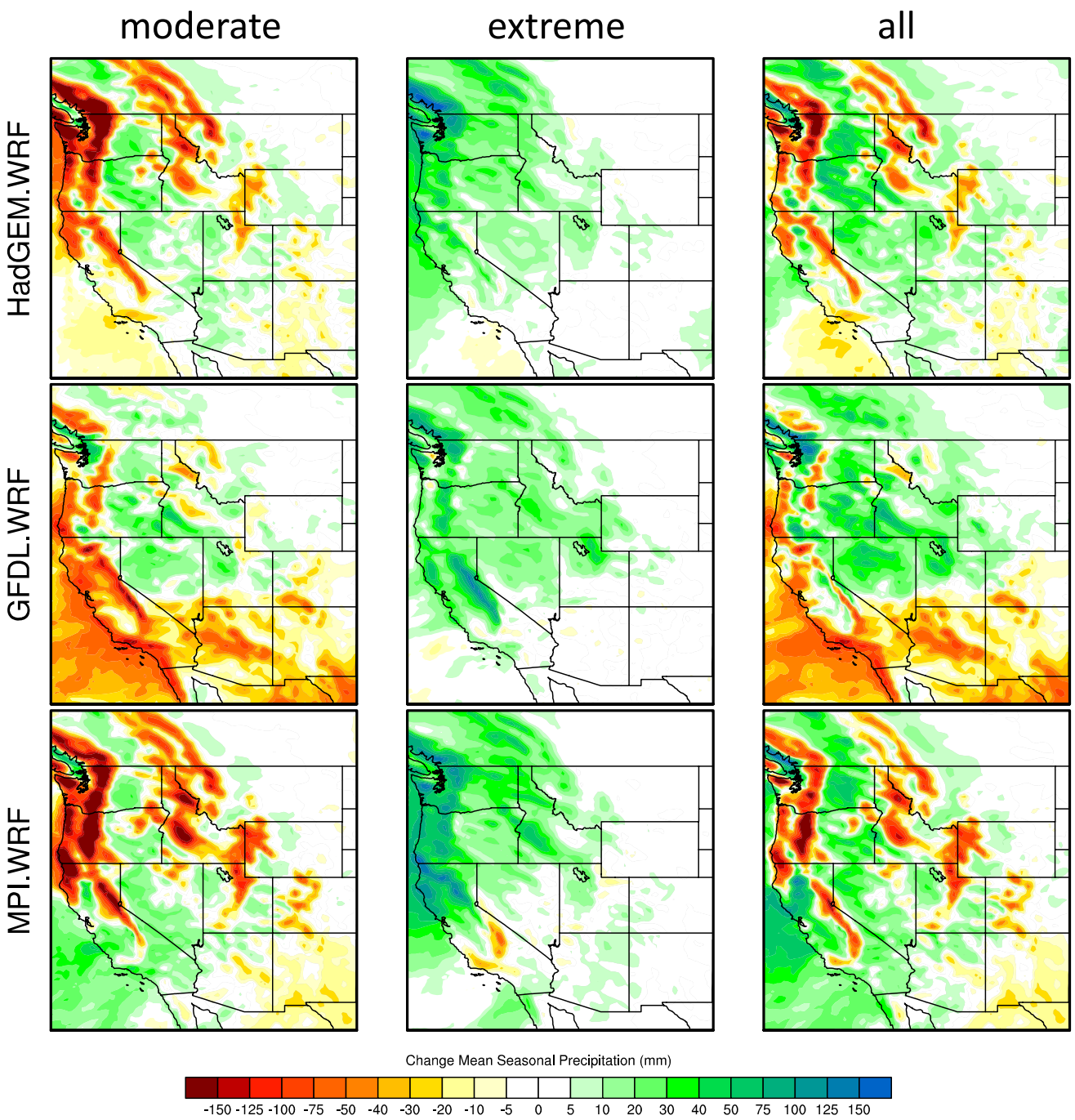

Fig. 10 Change (future–historical) in mean seasonal precipitation from (left) moderate IVT events, (center) extreme IVT events, and (right) all IVT events in (top) HadGEM.WRF, (middle) GFDL.WRF, and (bottom) MPI.WRF in 25 km WRF simulations

IVT-event-related precipitation changes are calculated for each month and watershed of Fig. 2, the changes in 'all' IVT-events (Figure S8) closely resemble the climatological monthly shifts in precipitation (Fig. 2).

Finally, to identify if localized projected IVT-event precipitation changes are related to the terrain elevation, we examine the changes in IVT-event total precipitation binned by elevation (Fig. 11). This analysis is similar to that of Fig. 3 except for IVT-event precipitation only. Figure 11 reveals another behavior that is consistent across all three simulations: large decreases in high-elevation, moderate IVT-event precipitation. This figure also helps explain why GFDL.WRF's cool season total precipitation change is statistically indistinguishable at low- and high-elevations (Fig. 3; notably it is the only ~ 25 km NA-CORDEX simulation with this behavior). As in MPI.WRF and HadGEM.WRF, GFDL.WRF's moderate IVT-event

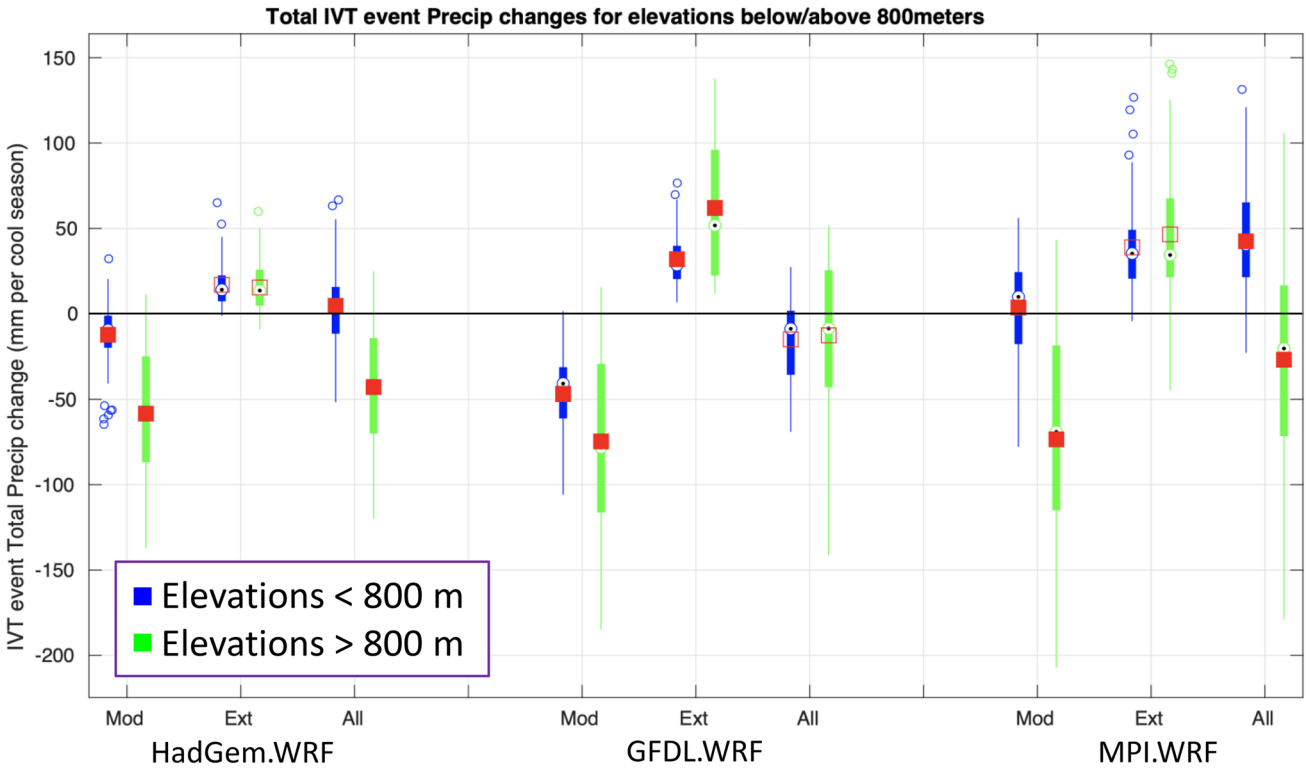

Fig. 11 IVT event total precipitation changes (normalized to mm per cool season) in the two California watersheds for 25 km HadGEM. WRF, GFDL.WRF, and MPI.WRF. Each model has three pairs of two box/whisker plots, corresponding to the results for Moderate (left pair), Extreme (middle pair), and All (right pair) IVT events. As in Fig. 3, the left (blue boxes) in each pair is gridpoints with elevations below 800 m and the right (green boxes) is gridpoints with elevations above 800 m. Open circles with black dots show median, boxes show 25/75 percentiles, whiskers extend to data points not considered outliers and small open circles show outliers. Red squares show means and are filled in for pairs that have significantly different means using a 2-sided t-test with 95% confidence intervals

precipitation decreases more at high- than low-elevation gridpoints. However, its extreme IVT-event precipitation increases everywhere, and significantly more at high elevations than at low elevations. The net result is GFDL.WRF exhibits no elevation dependence in its slightly negative, 'all' IVT-event precipitation change. In contrast, in HadGEM.WRF and MPI.WRF, the moderate IVT-event high-elevation precipitation reductions (relative to the low-elevation changes) are not offset by changes in extreme IVT-event precipitation, which are statistically indistinguishable at high and low elevations (although in both cases slightly positive, shifting up the 'All' IVT-event precipitation changes). We also note that the differences between Fig. 3 and the 'All' IVT-event columns in Fig. 11 is somewhat larger in GFDL.WRF than for the other two WRF simulations. This implies that the non-IVT-event precipitation is somewhat larger in GFDL.WRF.

4 Discussion

In the previous section, we examined how precipitation and IVT are projected to change across the WUS in NA-CORDEX simulations from both a seasonal perspective and through an examination of IVT-events as a step towards understanding the physical reasons for the projected changes. In this section, we frame these results with a discussion focused on the mechanisms potentially causing projected precipitation changes. We note that some of this discussion is speculative, and focus our discussion on the three watersheds of Fig. 2. We then follow with discussion of how these results fit into the existing literature on WUS precipitation and AR changes, and end with describing some implications and limitations of our study.

4.1 Relating precipitation changes to changes in IVT and smaller scale factors

We frame our discussion using the mechanisms primarily responsible for controlling precipitation in this region, ordered from larger scale (e.g., relating to IVT-event frequency, magnitude, and duration) to smaller scale (e.g., relating to mesoscale and microscale aspects of these phenomena). First, we discuss the IVT-event results and their relationship to precipitation amounts: the number of events per season of Fig. 7 is a measure of IVT-event frequency (given minimum event duration of 24 h) whereas the number of times per event of Table 2 combines both event frequency and duration (i.e., 36-h-long events would count as 1 event on Fig. 7, but 12 times in Table 2). For the three NA-CORDEX RCMs, we see somewhat consistent changes in IVT-event characteristics: more extreme IVT-events (and a net increase in frequency and duration), fewer moderate IVT-events, and increased composite event intensity (i.e., larger composite IVT, with greater increases for extreme IVT-events). The more frequent extreme IVT-events and larger event IVT for both event categories would act to increase total precipitation amounts whereas fewer moderate IVT-events would decrease total precipitation amounts, given unchanged precipitation efficiency during these events.

While we do not explicitly test the impact on precipitation of different mesoscale and microscale mechanisms for the NA-CORDEX WRF simulations (because these mechanisms require very high temporal resolution 3D atmospheric output that is computationally prohibitive to process), the composite IVT-event precipitation rate maps provide some insight into the net effect of smaller scale mechanisms combined with the impact of IVT-event intensity changes.

IVT-event precipitation changes for the CA watersheds are somewhat complex, but a few consistent patterns emerge (Figs. 9 and 10). First, focusing on extreme IVT-events: the southward-shifted, more zonal, more intense IVT distribution for the GFDL.WRF composite possibly explains the Sierra Nevada increases and northern and southern CA decreases in precipitation rate during these events, since the regions of increased (decreased) precipitation align with locations of strongest (weakest) IVT increase. Likewise, the more southwesterly orientation and large increase in IVT in HadGEM.WRF and MPI.WRF extreme IVT-events seem consistent with the precipitation rate increases along the northwestern Sierra Nevada and northern CA, OR, and WA coasts. The rather large precipitation rate differences across the Sierra Nevada in HadGEM.WRF could relate to the change in IVT orientation, but they are large enough to suggest that other meso- and microscale processes also play a role determining the precipitation change signal for these cases; more detailed analyses including investigations of microphysical processes (not available from these simulations, which incidentally use rather simple one-moment microphysics parameterizations) would be necessary to confirm these mechanisms. Despite the decreases in precipitation rate visible in the extreme IVT-event composites, the total change in precipitation from these events is generally positive, indicating the increase in the frequency and duration of these events is enough to compensate for the decreases in precipitation rate. The moderate IVT-event precipitation rate changes are generally fairly small positive in the Sierra Nevada (Fig. 9). However, when the precipitation is aggregated for moderate events large decreases at higher elevations are visible (Figs. 10 and 11). This shift from increases in precipitation rates to decreases in total precipitation suggests that the decreased number of moderate events is a primary cause of the total precipitation decreases.

All three simulations show slightly increased precipitation in the CNDB for both moderate and extreme IVT-events. We speculate that these precipitation rate increases in the CNDB could arise from two mechanisms that work in the same direction: the increased intensity of future IVT-events would result in more water being available for precipitation in the CNDB, and thus would act to increase CNDB precipitation if other factors remain unchanged. In addition, the precipitation efficiency of storms moving across the coastal mountains and Sierra Nevada into the CNDB might also decrease for future storms (Eidhammer et al. 2018). This efficiency is impacted by both microphysical and thermodynamic processes, both of which have been shown to change under warmer climate conditions. Thermodynamically, a decrease in condensational efficiency results from the Clausius–Clapyron-governed change in moisture with altitude (Kirshbaum and Smith 2008; Siler and Roe 2014). Cloud microphysical processes could also contribute to decreases in precipitation efficiency. For example, a shift from snow-dominated processes to rain-dominated processes (as might be expected in a generally warmer climate, e.g., Kirshbaum and Smith 2008, Sandvik et al. 2018, or Prein and Heymsfield 2020), results in less efficient conversion from condensate to precipitation. However, other studies have indicated increased precipitation efficiency from microphysical effects (e.g., higher fall speeds because of a shift from snow- to rain-dominated precipitation; Rasmussen et al. 2011), and these microphysical effects are likely sensitive to their parameterization (Colle 2004). The ambiguity in the microphysical impact on precipitation efficiency requires more research that is beyond the scope of this manuscript. Nevertheless, reduced precipitation efficiency along the Sierra Nevada and other upwind mountains would result in a smaller percentage of incoming IVT falling out prior to the airmass reaching the CNDB, resulting in more water available for precipitation in this interior basin.

Finally, we relate the changes in IVT-events back to the cool season mean and seasonal changes presented earlier in

the manuscript. The cool season total precipitation change patterns most closely resemble the 'total' IVT-event precipitation changes, which are a combination of (broadly) high elevation decreases during moderate IVT-events and widespread increases from extreme IVT-events. Across the Sierra Nevada, although extreme IVT-events increase in frequency resulting in more total precipitation, the reduction in moderate IVT-events and their reduced Sierra Nevada precipitation results in a net decreased cool season precipitation across the Sierra Nevada for the three RCMs investigated in detail. Although IVT-events generate a slightly smaller fraction of cool season precipitation for the CNDB than the Sierra Nevada, both moderate and extreme IVT-events have increased precipitation in the CNDB, consistent with the cool season precipitation increases for this region.

4.2 Relationship to previous results

As noted in the introduction, several publications have investigated projected changes in ARs at the end of the twenty-first century in both CMIP3 and CMIP5; on the whole, these studies have found increases in either frequency and/or intensity (with some differences based on how the events are defined, see review by Payne et al. (2020) and Table S1 for a summary of results from various manuscripts). Most existing definitions of ARs would include many of our moderate and extreme IVT-events, since they use IVT thresholds comparable to the 90th percentile lower threshold for our moderate IVT-events. Most AR literature does not investigate changes in different classes of ARs or in non-ARs (e.g. cutoff lows), although Rhoades et al. (2021) examines changes across AR categories (per Ralph et al. 2019a) and finds a projected reduction in Cat1-2 ARs and increase in Cat4-5 ARs, similar to our results. Moreover, our composites also include events that would likely fail objective length and width requirements used in many AR objective tools, and few studies have been done on non-AR changes: Gershunov et al. 2019 find a decrease in 'non-AR' precipitation (along with an increase in 'AR' precipitation), although they do not relate it to a change in the frequency, intensity, duration or precipitation efficiency of 'non-AR' storms. Given these nuances, and the wide variations across projected changes in ARs that depend on AR objective identification criterion, our results for the three RCMs are at least somewhat consistent with these previous results, particularly the increase we identify in both frequency and intensity of the most extreme IVT-events (analogous to extreme ARs).

WUS cool season precipitation change has also been widely investigated in previous studies. Overall most GCMs project end-of-century precipitation increases for the northwestern U.S., decreases for at least a few southwestern states, with zero mean change in between; the latitude of the change in sign in projected precipitation varies across GCMs. At lower elevations, the patterns of precipitation changes in the NA-CORDEX ensemble is broadly consistent with projected changes from GCMs. However, at higher elevations, NA-CORDEX WRF simulations project cool season decreases at many locations across the WUS, which here we've related to changes in the frequency, duration, intensity and precipitation efficiency of IVT-events. Other RCM studies (including those that use GCMs as their lateral boundary conditions like NA-CORDEX—e.g., Diffenbaugh et al. 2005; Wehner 2013; Rupp et al. 2017—and those that use alternative forcing approaches like a pseudo-global warming framework, e.g., Liu et al. 2017), also find projected precipitation increases in the lee of the Sierra Nevada and Cascade mountains. While few of these RCM studies project the decreases at high elevations we show exist in several of the NA-CORDEX simulations, some exhibit smaller fractional increases at high elevation (e.g., Mearns et al. 2013; Liu et al. 2017; Rupp et al. 2017).

4.3 Limitations and implications

End of century projections of western US precipitation are quantitatively still very uncertain, due to several factors which ultimately conspire to confound our confidence in such projections, such as large natural variability, and model disagreement on the location of the boundary between mid-latitude increases and subtropical decreases in precipitation (Neelin et al. 2013; Tebaldi et al. 2011). These issues are further complicated by the smaller GCM sample in NA-CORDEX than in CMIP5, and the regional variability introduced by the RCMs. The relatively small GCM sample of NA-CORDEX is particularly relevant for our understanding of climate projections because, as noted in Meyer et al. (2021) and Mahoney et al. (2021), the GCM-driver plays a key role in the climate change signal of the NA-CORDEX simulations. In addition, we were able to test changes in IVT-events in only three of the NA-CORDEX RCMs with high temporal-resolution 3D output available, limiting the simulations for which physical explanations of precipitation changes were available.

While IVT-events are likely reasonably well captured by GCMs, the meso- and microscale processes responsible for determining precipitation amounts at high elevation during IVT-events are not well represented in GCMs, thus changes in these orographic precipitation processes might be totally absent (i.e., GCMs might miss the non-linearity of these changes, e.g., slight increases in event IVT but decreases in precipitation efficiency). While NA-CORDEX better-resolves the mountainous WUS than most GCMs, several manuscripts have documented the benefit of even higher resolution, convection-permitting models (CPMs) for climate change simulations (Liu et al. 2017; Berthou et al. 2020; Prein et al. 2015). CPMs potentially improve upon the

fidelity of the physics in regional simulations at coarser resolutions (e.g., NA-CORDEX) through their higher resolution which allows the elimination of a convective parameterization, but to date their computational cost still prohibits multi-decadal, multi-model ensembles (e.g., Gutowski et al. 2020).

Our results are bolstered by a few factors. First is the broad consistency with previous work (as noted in the previous section). Second, even though IVT-events could be investigated in only three RCMs, several of the other RCMs exhibited similar high elevation precipitation decreases, albeit in varying locations across the WUS, suggesting this mechanism might be present in a substantial portion of NA-CORDEX simulations. Third, there's limited evidence that as GCMs move to higher resolution, similar features of reduced precipitation across higher WUS terrain might appear (Fig. 14.18 in IPCC chapter 14), and as noted in the previous section some evidence of at least smaller fractional increases at high elevations in other RCMs. This result suggests that further investment into higher resolution climate models, both global and regional in scale, that better resolve orographic precipitation processes, is warranted to better constrain projections of precipitation in areas of complex topography (e.g., Roberts et al. 2018).

Finally, this manuscript has focused on total precipitation and documents projected decreases in high elevation precipitation. However, a significant fraction of precipitation that falls across the mountainous western US arrives as snow, and contributes to seasonal snowpack, which supports water supply and allocation decisions into the spring. Given rising temperatures, snowpack might be expected to decline even in the face of no change of precipitation, and here we've shown that precipitation decreases at some high elevation locations. Mahoney et al. (2021) demonstrate large reductions in snowpack in NA-CORDEX simulations. This reduced snow water storage, combined with a shortening of the precipitation season and increases in extreme IVT-events, points to a future where it is more difficult to manage water in the WUS.

5 Conclusion/summary

This manuscript investigates end-of-21st-century projections of western US precipitation and IVT in a collection of regional climate models (RCMs) forced by several global climate models (GCMs) from the North American Coordinated Regional climate Downscaling Experiment (NA-CORDEX). Several of the NA-CORDEX RCMs project a decrease in cool season precipitation at high elevation (e.g., across the Sierra Nevada) with a corresponding increase in the Great Basin of the US. How these terrain-related precipitation changes relate to changes in IVT and IVT-events is explored in a subset of the NA-CORDEX RCMs. We find that extreme IVT-events increase in frequency. In contrast, moderate IVT-events decrease in frequency. These results are somewhat consistent with previous work since most previous investigations of ARs in a changing climate do not subdivide ARs by their intensity.

We then relate the changes in IVT-events to the projected precipitation changes. For the CNDB, precipitation during IVT-events generally increases regardless of IVT-event intensity. However, for the Sierra Nevada, the precipitation response depends on IVT-event intensity. Extreme IVT-events generally show an end-of-century increase in precipitation across the Sierra Nevada; in contrast, precipitation during moderate IVT-events generally decreases across the Sierra Nevada. Thus, we argue that the mean cool season decrease at high elevation is largely determined by the projected decrease in moderate IVT-events which are also projected to generate less high elevation precipitation.

The NA-CORDEX projected reduction in high elevation precipitation, when paired with a shortening of the wet season across California that several other manuscripts have demonstrated, points to a CA whose water years are more variable and volatile, with even more difficult-to-manage water resources.

Supplementary Information The online version contains supplementary material available at https://doi.org/10.1007/s00382-022-06168-6.

Funding This work was supported by grants from the following: (1) the US Bureau of Reclamation Science & Technology office (PI: Mike Wright, Mid-Pacific Region), (2) the Strategic Environmental Research and Development Program (SERDP) and Environmental Security Technology Certification Program (ESTCP) through grant RC-201666, and (3) the U.S. Department of Energy, Office of Science, Office of Biological and Environmental Research program under Award Numbers DE-SC0016605 and DE-SC0016438. Additionally, NCAR is sponsored by the NSF under Cooperative Agreement No. 1852977. We would like to thank the other members of NCAR's NA-CORDEX team, in particular L. Mearns and S. McGinnis, for their mentoring of the NA-CORDEX dataset and project. We would also like to thank W. Ryan Currier and three anonymous reviewers whose comments and suggestions greatly improved the manuscript.Regarding NA-CORDEX: We acknowledge the World Climate Research Programme's Working Group on Regional Climate, and the Working Group on Coupled Modelling, former coordinating body of CORDEX and responsible panel for CMIP5. We also thank the climate modelling groups (listed in http://na-cordex.org/simulations-modeling-group.html) for producing and making available their model output. We also acknowledge the U.S. Department of Defense ESTCP for its support of the NA-CORDEX data archive. Regarding CMIP5: we acknowledge the World Climate Research Programme's Working Group on Coupled Modelling, which is responsible for CMIP, and we thank the climate modeling groups for producing and making available their model output. For CMIP the U.S. Department of Energy's Program for Climate Model Diagnosis and Intercomparison provides coordinating support and led development of software infrastructure in partnership with the Global Organization for Earth System Science Portals.

Data and code availability Precipitation for both NA-CORDEX and CMIP5 are publicly available. CMIP5 precipitation and temperature

data are available to download from the World Climate Research Program at https://esgf-node.llnl.gov/search/cmip5/ or to visually explore on https://psl.noaa.gov/ipcc/cmip5/. NA-CORDEX precipitation and temperature data can be downloaded from NCAR's Climate Data Gateway at https://www.earthsystemgrid.org/search/cordexsearch.html. The IVT dataset generated and analyzed during this study, as well as analysis software, are available from the corresponding author on reasonable request.

Declarations

Conflict of interest The authors declare they have no conflict of interest.

References

Abatzoglou JT (2016) Contribution of cutoff lows to precipitation across the United States*. J Appl Meteorol Climatol 55:893–899

Bengtsson L, Hodges KI, Roeckner E (2006) Storm tracks and climate change. J Clim 19(15):3518–3543. Retrieved 10 Feb 2022. https://journals.ametsoc.org/view/journals/clim/19/15/jcli3815.1.xml

Berthou S, Kendon EJ, Chan SVC, Ban NI, Leutwyler D, Schar C, Fosser G (2020) Pan-European climate at convection-permitting scale: a model intercomparison study. Clim Dyn 55:35–59

Bukovsky MS, Mearns LO (2020) Regional climate change projections from NA-CORDEX and their relation to climate sensitivity. Clim Change 162:645–665

Chang EKM, Guo YJ, Xia XM (2012) CMIP5 multimodel ensemble projection of storm track change under global warming. J Geophys Res Atmos 117

Colle BA (2004) Sensitivity of orographic precipitation to changing ambient conditions and terrain geometries: an idealized modeling perspective. J Atmos Sci 61:588–606

Deser C, Phillips A, Bourdette V, Teng HY (2012) Uncertainty in climate change projections: the role of internal variability. Clim Dyn 38:527–546

Dettinger M (2011) Climate change, atmospheric rivers, and floods in California—a multimodel analysis of storm frequency and magnitude changes. J Am Water Resour Assoc 47:514–523

Dettinger MD, Ralph FM, Das T, Neiman PJ, Cayan DR (2011) Atmospheric rivers, floods and the water resources of California. Water 3:445–478

Diffenbaugh NS, Pal JS, Trapp RJ, Giorgi F (2005) Fine-scale processes regulate the response of extreme events to global climate change. Proc Natl Acad Sci USA 102:15774–15778

Eidhammer T, Grubisic V, Rasmussen R, Ikdea K (2018) Winter precipitation efficiency of mountain ranges in the Colorado rockies under climate change. J Gerontol Ser A Biol Med Sci 123:2573–2590

Fyfe JC, Derksen C, Mudryk L, Flato GM, Santer BD, Swart NC, Molotch NP, Zhang XB, Wan H, Arora VK, Scinocca J, Jiao YJ (2017) Large near-term projected snowpack loss over the western United States. Nat Commun 8

Gao Y, Lu J, Leung R, Yang Q, Hagos S, Qian Y (2015) Dynamical and thermodynamical modulations on future changes of landfalling atmospheric rivers over western North America. Geophys Res Lett 42:7179–7186

Gershunov A, Shulgina T, Clemesha RES, Guirguis K, Pierce DW, Dettinger MD, Lavers DA, Cayan DR, Polade SD, Kalansky J, Ralph FM (2019) Precipitation regime change in Western North America: the role of Atmospheric Rivers. Sci Rep 9

Gibson PB, Waliser DE, Lee H, Tian BJ, Massoud E (2019) Climate model evaluation in the presence of observational uncertainty: precipitation indices over the contiguous United States. J Hydrometeorol 20:1339–1357

Giorgi F, Jones C, Asrar GR (2009) Addressing climate information needs at the regional level: the CORDEX framework. WMO Bull 58:175

Gonzales KR, Swain DL, Barnes EA, Diffenbaugh NS (2020) Moisture-versus wind-dominated flavors of atmospheric rivers. Geophys Res Lett 47

Gutowski WJ, Giorgi F, Timbal B, Frigon A, Jacob D, Kang HS, Raghavan K, Lee B, Lennard C, Nikulin G, O'Rourke E, Rixen M, Solman S, Stephenson T, Tangang F (2016) WCRP COordinated Regional Downscaling EXperiment (CORDEX): a diagnostic MIP for CMIP6. Geosci Model Dev 9:4087–4095

Gutowski WJ, Ullrich PA, Hall A, Leung LR, O'Brien TA, Patricola CM, Arritt RW, Bukovsky MS, Calvin KV, Feng Z, Jones AD, Kooperman GJ, Monier E, Pritchard MS, Pryor SC, Qian Y, Rhoades AM, Roberts AF, Sakaguchi K, Urban N, Zarzycki C (2020) The ongoing need for high-resolution regional climate models: process understanding and stakeholder information. Bull Am Meteor Soc 101:E664–E683

Hecht CW, Cordeira JM (2017) Characterizing the influence of atmospheric river orientation and intensity on precipitation distributions over North Coastal California. Geophys Res Lett 44:9048–9058

Henn B, Clark MP, Kavetski D, Newman AJ, Hughes M, McGurk B, Lundquist JD (2018) Spatiotemporal patterns of precipitation inferred from streamflow observations across the Sierra Nevada mountain range. J Hydrol 556:993–1012

Hughes M, Neiman PJ, Sukovich E, Ralph M (2012) Representation of the Sierra Barrier Jet in 11 years of a high-resolution dynamical reanalysis downscaling compared with long-term wind profiler observations. J Geophys Res Atmos 117

Hughes M, Mahoney KM, Neiman PJ, Moore BJ, Alexander M, Ralph FM (2014) The landfall and inland penetration of a flood-producing atmospheric river in Arizona. Part II: sensitivity of modeled precipitation to terrain height and atmospheric river orientation. J Hydrometeorol 15:1954–1974

Hughes M, Lundquist J, Henn B (2017) Dynamical downscaling improves upon gridded precipitation products in the Sierra Nevada, California. Clim Dyn 55:111

IPCC (2014) Climate change 2013: the physical science basis:1–1535

Kirshbaum DJ, Smith RB (2008) Temperature and moist-stability effects on midlatitude orographic precipitation. Q J R Meteorol Soc 134:1183–1199

Knowles N, Dettinger MD, Cayan DR (2006) Trends in snowfall versus rainfall in the Western United States. J Clim 19:4545–4559

Langenbrunner B, Neelin JD (2017) Pareto-optimal estimates of California precipitation change. Geophys Res Lett 44:12436–12446

Lavers DA, Ralph FM, Waliser DE, Gershunov A, Dettinger MD (2015) Climate change intensification of horizontal water vapor transport in CMIP5. Geophys Res Lett 42:5617–5625

Liu CH, Ikeda K, Rasmussen R, Barlage M, Newman AJ, Prein AF, Chen F, Chen L, Clark M, Dai AG, Dudhia J, Eidhammer T, Gochis D, Gutmann E, Kurkute S, Li YP, Thompson G, Yates D (2017) Continental-scale convection-permitting modeling of the current and future climate of North America. Clim Dyn 49:71–95

Lundquist J, Hughes M, Gutmann E, Kapnick S (2019) Our skill in modeling mountain rain and snow is bypassing the skill of our observational networks. Bull Am Meteor Soc 100:2473–2490

Mahoney K, Scott JD, Alexander M, McCrary R, Hughes M, Swales D, Bukovsky M (2021) Cool season precipitation projections for California and the Western United States in NA-CORDEX. Clim Dyn 56:9–10

Martin AC, Ralph FM, Wilson A, DeHaan L, Kawzenuk B (2019) Rapid cyclogenesis from a mesoscale frontal wave on an

atmospheric river: impacts on forecast skill and predictability during atmospheric river landfall. J Hydrometeorol 20:1779–1794
McCrary R, Mearns LO, Hughes M, Biner S, Bukovsky M (2021) Projections of North American snow from NA-CORDEX and their uncertainties, with a focus on model resolution. Clim Change **(in review)**
McGinnis S, Mearns LO (2021) Building a climate service for North America based on the NA-CORDEX data archive. Geosci Model Dev 22:100233
Mearns LO, Sain S, Leung LR, Bukovsky MS, McGinnis S, Biner S, Caya D, Arritt RW, Gutowski W, Takle E, Snyder M, Jones RG, Nunes AMB, Tucker S, Herzmann D, McDaniel L, Sloan L (2013) Climate change projections of the North American Regional Climate Change Assessment Program (NARCCAP). Clim Change 120:965–975
Mearns LO, McGinnis S, Korytina D, Arritt R, Biner S, Bukovsky M, Chang HI, Christensen O, Herzmann D, Jiao Y (2017) The NA-CORDEX dataset, version 1.0. NCAR Climate Data Gateway. The North American CORDEX Program 10:D6SJ1JCH, Boulder
Meyer JDD, Wang SYS, Gillies RR, Yoon JH (2021) Evaluating NA-CORDEX historical performance and future change of western US precipitation patterns and modes of variability. Int J Climatol 41:4509–4532
Mote PW, Hamlet AF, Clark MP, Lettenmaier DP (2005) Declining mountain snowpack in western North America. Bull Am Meteorol Soc 86:39
Mundhenk BD, Barnes EA, Maloney ED (2016) All-season climatology and variability of atmospheric river frequencies over the North Pacific. J Clim 29:4885–4903
Neelin JD, Langenbrunner B, Meyerson JE, Hall A, Berg N (2013) California winter precipitation change under global warming in the coupled model intercomparison project phase 5 ensemble. J Clim 26:6238–6256
Neiman PJ, Ralph FM, Wick GA, Lundquist JD, Dettinger MD (2008) Meteorological characteristics and overland precipitation impacts of atmospheric rivers affecting the West Coast of North America based on eight years of SSM/I satellite observations. J Hydrometeorol 9:22–47
Newman AJ, Clark MP, Craig J, Nijssen B, Wood A, Gutmann E, Mizukami N, Brekke L (2015) Gridded ensemble precipitation and temperature estimates for the contiguous United States. J Hydrometeorol 16:2481–2500
Payne AE, Magnusdottir G (2015) An evaluation of atmospheric rivers over the North Pacific in CMIP5 and their response to warming under RCP 8.5. J Gerontol Ser A Biol Med Sci 120:11173–11190
Payne AE, Demory M-E, Leung LR, Ramos AM, Shields CA, Rutz JJ, Siler N, Villarini G, Hall A, Ralph FM (2020) Responses and impacts of atmospheric rivers to climate change. Nat Rev Earth Environ 1:143–157
Picard L, Mass C (2017) The sensitivity of orographic precipitation to flow direction: an idealized modeling approach. J Hydrometeorol 18:1673–1688
Prein AF, Heymsfield AJ (2020) Increased melting level height impacts surface precipitation phase and intensity. Nat Clim Change 10:771
Prein AF, Langhans W, Fosser G, Ferrone A, Ban N, Goergen K, Keller M, Tolle M, Gutjahr O, Feser F, Brisson E, Kollet S, Schmidli J, van Lipzig NPM, Leung R (2015) A review on regional convection-permitting climate modeling: demonstrations, prospects, and challenges. Rev Geophys 53:323–361
Prein AF, Bukovsky MS, Mearns LO, Bruyere CL, Done JM (2019) Simulating North American weather types with regional climate models. Front Environ Sci 7
NOAA PSL (2021) CORDEX precipitation analysis. https://psl.noaa.gov/ipcc/cordex/
Radic V, Cannon AJ, Menounos B, Gi N (2015) Future changes in autumn atmospheric river events in British Columbia, Canada, as projected by CMIP5 global climate models. J Gerontol Ser A Biol Med Sci 120:9279–9302
Ralph FM, Neiman PJ, Wick GA, Gutman SI, Dettinger MD, Cayan DR, White AB (2006) Flooding on California's Russian River: role of atmospheric rivers. Geophys Res Lett 33
Ralph FM, Rutz JJ, Cordeira JM, Dettinger M, Anderson M, Reynolds D, Schick LI, Smallcomb C (2019a) A scale to characterize the strength and impacts of atmospheric rivers. Bull Am Meteor Soc 100:269–290
Ralph FM, Wilson AM, Shulgina T, Kawzenuk B, Sellars S, Rutz JJ, Lamjiri MA, Barnes EA, Gershunov A, Guan B (2019b) ARTMIP-early start comparison of atmospheric river detection tools: how many atmospheric rivers hit northern California's Russian River watershed? Clim Dyn 52:4973–4994
Rasmussen R, Liu CH, Ikeda K, Gochis D, Yates D, Chen F, Tewari M, Barlage M, Dudhia J, Yu W, Miller K, Arsenault K, Grubisic V, Thompson G, Gutmann E (2011) High-resolution coupled climate runoff simulations of seasonal snowfall over Colorado: a process study of current and warmer climate. J Clim 24:3015–3048
Reeves HD, Lin YL, Rotunno R (2008) Dynamic forcing and mesoscale variability of heavy precipitation events over the Sierra Nevada mountains. Mon Weather Rev 136:62–77
Rhoades AM, Jones AD, Srivastava A, Huang HP, O'Brien TA, Patricola CM, Ullrich PA, Wehner M, Zhou Y (2020) The shifting scales of Western US landfalling atmospheric rivers under climate change. Geophys Res Lett 47
Rhoades AM, Risser MD, Stone DA, Wehner MF, Jones AD (2021) Implications of warming on western United States landfalling atmospheric rivers and their flood damages. Weather Clim Extrem 32
Roberts MJ, Vidale PL, Senior C, Hewitt HT, Bates C, Berthou S, Chang P, Christensen HM, Danilov S, Demory ME, Griffies SM, Haarsma R, Jung T, Martin G, Minobe S, Ringler T, Satoh M, Schiemann R, Scoccimarro E, Stephens G, Wehner MF (2018) The benefits of global high resolution for climate simulation: process understanding and the enabling of stakeholder decisions at the regional scale. Bull Am Meteor Soc 99:2341–2359
Roe GH (2005) Orographic precipitation. Annu Rev Earth Planet Sci 33:645–671
Rupp DE, Li SH, Mote PW, Shell KM, Massey N, Sparrow SN, Wallom DCH, Allen MR (2017) Seasonal spatial patterns of projected anthropogenic warming in complex terrain: a modeling study of the western US. Clim Dyn 48:2191–2213
Rutz JJ, Steenburgh WJ (2012) Quantifying the role of atmospheric rivers in the interior western United States. Atmos Sci Lett 13:257–261
Rutz JJ, Steenburgh WJ, Ralph FM (2014) Climatological characteristics of atmospheric rivers and their inland penetration over the Western United States. Mon Weather Rev 142:905–921
Rutz JJ, Shields CA, Lora JM, Payne AE, Guan B, Ullrich P, O'Brien T, Leung LR, Ralph FM, Wehner M, Brands S, Collow A, Goldenson N, Gorodetskaya I, Griffith H, Kashinath K, Kawzenuk B, Krishnan H, Kurlin V, Lavers D, Magnusdottir G, Mahoney K, McClenny E, Muszynski G, Nguyen PD, Prabhat QY, Ramos AM, Sarangi C, Sellars S, Shulgina T, Tome R, Waliser D, Walton D, Wick G, Wilson AM, Viale M (2019) The atmospheric river tracking method intercomparison project (ARTMIP): quantifying uncertainties in atmospheric river climatology. J Gerontol Ser A Biol Med Sci 124:13777–13802
Sandvik MI, Sorteberg A, Rasmussen R (2018) Sensitivity of historical orographically enhanced extreme precipitation events to idealized temperature perturbations. Clim Dyn 50:143–157

Schwalm CR, Glendon S, Duffy PB (2020) RCP8.5 tracks cumulative CO_2 emissions. Proc Natl Acad Sci USA 117:19656–19657

Sellars S, Nguyen P, Chu W, Gao X, Hsu K-l, Sorooshian S (2013) Computational Earth science: Big data transformed into insight. EOS Trans Am Geophys Union 94:277–278

Shields CA, Kiehl JT (2016) Atmospheric river landfall-latitude changes in future climate simulations. Geophys Res Lett 43:8775–8782

Shields CA, Rutz JJ, Leung LR, Ralph FM, Wehner M, O'Brien T, Pierce R (2019) Defining uncertainties through comparison of atmospheric river tracking methods. Bull Am Meteorol Soc 100:ES93–ES96

Siler N, Roe G (2014) How will orographic precipitation respond to surface warming? An idealized thermodynamic perspective. Geophys Res Lett 41:2606–2613

Smith RB (2003) A linear upslope-time-delay model for orographic precipitation. J Hydrol 282:2–9

Smith SA, Vosper SB, Field PR (2015) Sensitivity of orographic precipitation enhancement to horizontal resolution in the operational Met Office Weather forecasts. Meteorol Appl 22(1):14–24

Swain DL, Langenbrunner B, Neelin JD, Hall A (2018) Increasing precipitation volatility in twenty-first-century California. Nat Clim Change 8:427

Taylor KE, Stouffer RJ, Meehl GA (2012) An overview of CMIP5 and the experiment design. Bull Am Meteor Soc 93:485–498

Tebaldi C, Arblaster JM, Knutti R (2011) Mapping model agreement on future climate projections. Geophys Res Lett 38

Torma C, Giorgi F, Coppola E (2015) Added value of regional climate modeling over areas characterized by complex terrain precipitation over the Alps. J Gerontol Ser A Biol Med Sci 120:3957–3972

Us Geological Survey and Us Department of Agriculture NRCS (2013) Federal standards and procedures for the National Watershed Boundary Dataset (WBD). Tech Methods 11:63

USBR (2016) SECURE Water Act Section 9503(c)—reclamation climate change and water 2016

Warner MD, Mass CF, Salathe EP (2015) Changes in winter atmospheric rivers along the North American west coast in CMIP5 climate models. J Hydrometeorol 16:118–128

Wehner MF (2013) Very extreme seasonal precipitation in the NARCCAP ensemble: model performance and projections. Clim Dyn 40:59–80

Wuebbles D, Meehl G, Hayhoe K, Karl TR, Kunkel K, Santer B, Wehner M, Colle B, Fischer EM, Fu R, Goodman A, Janssen E, Kharin V, Lee H, Li WH, Long LN, Olsen SC, Pan ZT, Seth A, Sheffield J, Sun LQ (2014) CMIP5 climate model analyses climate extremes in the United States. Bull Am Meteor Soc 95:571–583

Wuebbles DJ, Fahey DW, Hibbard KA, Arnold JR, DeAngelo B, Doherty S, Easterling DR, Edmonds J, Edmonds T, Hall T (2017) Climate science special report: Fourth national climate assessment (NCA4), vol I